Uncertainty in Retrieving Raindrop Size Distribution from Polarimetric Radar Measurements

HAO HUANG

Key Laboratory for Mesoscale Severe Weather, Ministry of Education, and School of Atmospheric Sciences, Nanjing University, Nanjing, and State Key Laboratory of Severe Weather, and Joint Center for Atmospheric Radar Research, Centre of Modern Analysis, Nanjing University, Beijing, China

GUIFU ZHANG

School of Atmospheric Sciences, Nanjing University, Nanjing, China, and School of Meteorology, University of Oklahoma, Norman, Oklahoma

KUN ZHAO, SU LIU, LONG WEN, GANG CHEN, AND ZHENGWEI YANG

Key Laboratory for Mesoscale Severe Weather, Ministry of Education, and School of Atmospheric Sciences, Nanjing University, Nanjing, and State Key Laboratory of Severe Weather, and Joint Center for Atmospheric Radar Research, Centre of Modern Analysis, Nanjing University, Beijing, China

(Manuscript received 27 June 2018, in final form 25 December 2018)

ABSTRACT

Drop size distribution (DSD) is a fundamental parameter in rain microphysics. Retrieving DSDs from polarimetric radar measurements extends the capabilities of rain microphysics research and quantitative precipitation estimation. In this study, issues in rain DSD retrieval were studied with simulated and measured data. It was found that a three-parameter gamma distribution model was not suitable for directly retrieving DSD from polarimetric radar measurements. A statistical constraint, such as the shape–slope relation used in the constrained-gamma (C-G) distribution model, helped to reduce the uncertainties and errors in the retrieval. The inclusion of specific differential phase (K_{DP}) measurements resulted in more accurate DSD retrieval and rain physical parameter estimation if the measurement errors were properly characterized in the error minimization analysis (EMA), which was verified using two real precipitation events. The study demonstrated the potential of using full polarimetric radar measurements to improve rain DSD retrieval.

1. Introduction

Drop size distribution (DSD) is a fundamental property of rain microphysics. Rain DSD, denoted as $N(D)$, is defined as the numbers of raindrops in a unit volume per unit size bin (with unit $\mathrm{mm^{-1}\,m^{-3}}$). The sizes of raindrops are represented using the equivolume diameter D (mm). Different moments of $N(D)$ are used alone or combined to calculate physical and statistical parameters of rain, including rainfall rate R ($\mathrm{mm\,h^{-1}}$), liquid water content W ($\mathrm{g\,m^{-3}}$), mass-weighted mean diameter D_m (mm), and total number concentration N_t ($\mathrm{m^{-3}}$). Other parameters regarding these physical processes, for example, the evaporation rate and the accretion rate, are also related to DSDs (Zhang et al. 2006).

A disdrometer is an in situ instrument used to measure DSDs. A disdrometer usually has a limited sampling area, and the spatial and temporal variabilities of weather systems make it difficult to obtain comprehensive measurements of DSDs (Bringi et al. 2015). Polarimetric radars typically have fine spatiotemporal resolutions and large coverage, which can measure the microphysical properties of raindrops using horizontally and vertically polarized channels. The measurements made by polarimetric radars, namely, horizontal reflectivity factor Z_H (dBZ), differential reflectivity Z_{DR} (dB), and specific differential phase K_{DP} ($^\circ\,\mathrm{km^{-1}}$), are related to the DSDs (Cao et al. 2012). Therefore, it is possible to retrieve an estimated $N(D)$ from the

Corresponding author: Guifu Zhang, guzhang1@ou.edu; Kun Zhao, zhaokun@nju.edu.cn

DOI: 10.1175/JTECH-D-18-0107.1

polarimetric measurements. Because only three types of measurements (Z_H, Z_{DR}, and K_{DP}) are available for the quantitative retrieval, $N(D)$ should be represented using simplified DSD models containing only a few parameters. The gamma distribution $N(D) = N_0 D^{\mu} \exp(-\Lambda D)$, $D_{min} \le D \le D_{max}$ is widely used to represent natural rain spectra, where N_0 ($mm^{-1-\mu} m^{-3}$) is the number concentration parameter, μ (unitless) is the shape parameter, Λ (mm^{-1}) is the slope parameter, and D_{min} (mm) and D_{max} (mm) are the minimum and maximum diameters of raindrops respectively (Ulbrich 1983; Testud et al. 2001).

Because most DSD variabilities can be accounted for by a DSD model with 2 degrees of freedom (Morrison et al. 2019), the gamma distribution was usually further constrained for DSD retrieval. Seliga and Bringi (1976) proposed to calculate R and the median volume diameter D_0 (mm) from Z_H and Z_{DR} based on the exponential distribution, which assumes $\mu = 0$ in the gamma distribution. Zhang et al. (2001) used the gamma distribution constrained by a statistical relation between μ and Λ in retrieval, which was cross verified with the relation between D_m and the mass spectrum standard deviation σ_m (mm; Zhang et al. 2003; Moisseev and Chandrasekar 2007). Cao et al. (2008) also found that the μ–Λ relation may vary in different climate regions (Cao and Zhang 2009). With the constraint of the μ–Λ relation, the degrees of freedom in the gamma distribution is reduced to 2 for DSD retrieval. Testud et al. (2001) demonstrated that the average normalized DSD spectra with 2 degrees of freedom were stable. Later on, Lee et al. (2004) proposed to use a double-moment normalization method to express DSD as a combination of two DSD moments and a double-moment normalized function. Recently, this method was also adapted for X band (Raupach and Berne 2017). Williams et al. (2014) proposed the retrieval of DSD on the basis of the normalized gamma distribution constrained by a statistical relation between D_m and σ_m. In the Self-Consistent with Optimal Parameterization attenuation correction and Microphysics Estimation (SCOP-ME) algorithm, a statistical relation between D_0 and μ was used (Anagnostou et al. 2013; Kalogiros et al. 2013).

Using the DSD models with 2 degrees of freedom, the DSD parameters and $N(D)$ can be explicitly estimated from two measurements of rain; Z_H and Z_{DR} are usually chosen as the measurements. However, polarimetric radars also measure the differential phase Φ_{DP} and its derivative K_{DP}. Because K_{DP} is approximately proportional to the fourth moment of $N(D)$, it provides useful information about rain (Huang et al. 2017). Gorgucci et al. (2002) attempted to include K_{DP} for the estimation of D_0, N_w (the generalized intercept parameter for the normalized gamma distribution), and μ, as well as the shape of the raindrops, which is known as the beta method. However, the method proved to be unstable due to the errors in K_{DP} according to Brandes et al. (2004b). As a result, when adapting the method for X band, only the data with rainfall rates above 10 mm h^{-1} were used in the study of Park et al. (2005). This method was extended to reduce the impact of the measurement errors in Z_{DR} and K_{DP} in Bringi et al. (2002). Whether the inclusion of K_{DP} can improve the retrieval depends on whether useful information is utilized and the effect of measurement errors is reduced at the same time, which has not been comprehensively studied yet. With the inclusion of K_{DP}, there are three available measurements. The most instinctive way is to estimate DSD based on the gamma distribution, which has 3 degrees of freedom. Its feasibility and performance will be studied. Moreover, even when using a DSD model with 2 degrees of freedom (e.g., the gamma distribution constrained by a μ–Λ relation), K_{DP} can be incorporated using some mathematical methods, for example, the error minimization analysis (EMA), which will be described in later sections. We assessed the impact of K_{DP} measurements on DSD retrievals based on these models.

The methods used in this study are introduced in section 2. The feasibility and performance of DSD retrieval using the three-parameter gamma distribution (three-parameter GM) are given in section 3. The performance of the retrievals based on the exponential distribution (EXP) and the gamma distribution constrained by a μ–Λ relation [constrained gamma (C-G)] was used as a reference. A quantitative study of K_{DP}'s influences on DSD retrievals on the basis of EXP and C-G is presented in section 4. Section 5 presents a comparison of the performance of the DSD retrievals with and without K_{DP} measurements in a real weather event. The conclusions and further discussion are given in section 6.

2. Methods

According to Cao et al. (2012), the polarimetric variables (Z_H, Z_{DR}, and K_{DP}) are related to $N(D)$ via

$$Z_{H,V} = 10\log_{10}\left[\frac{4\lambda^4}{\pi^4|K_w|^2}\int_{D_{min}}^{D_{max}}|S_{h,v}(\pi, D)|^2 N(D)\,dD\right], \tag{1}$$

$$Z_{DR} = Z_H - Z_V, \tag{2}$$

$$K_{DP} = \frac{0.18\lambda}{\pi}\int_{D_{min}}^{D_{max}}\mathrm{Re}[s_h(0, D) - s_v(0, D)]N(D)\,dD, \tag{3}$$

where D (mm) is the equivalent diameters of the raindrops, λ (mm) is the radar wavelength, $K_w = (\varepsilon - 1)/(\varepsilon + 2)$ where ε (unitless) is the relative dielectric

constant of water, $s_{h,v}(\alpha, D)$ (mm) is the complex scattering amplitude at the horizontal or vertical polarization for raindrops of diameter D, with the parameter α being the angle between the incident and scattering directions (in radian), and $\mathrm{Re}(\cdot)$ means the real part of a complex number (Doviak and Zrnić 1993; Bringi and Chandrasekar 2001; Zhang et al. 2001; Cao et al. 2012). Note that the reflectivity factors in linear scale are in units of $\mathrm{mm}^6\,\mathrm{m}^{-3}$, and the Z_H and Z_V are the reflectivity factors in decibels. In this study, the scattering amplitudes were calculated with the T-matrix method (Vivekanandan et al. 1991; Mishchenko et al. 1996). The axis ratio relation was assumed to be the same as that from Brandes et al. (2002). Since the effect of raindrop oscillations has been taken into account in their axis ratio, no additional canting angle was considered in the simulation of our study. The environmental temperature was set to 20°C. The radar wavelength was assumed to be 10.7 cm, which is used by operational S-band radars. The $D_{\min}$ and $D_{\max}$ were usually assumed to be 0 and 8 mm respectively in the retrieval.

To retrieve rain DSDs from polarimetric radar data, a DSD model of two or three free parameters is needed in Eqs. (1)–(3). For example, if the gamma distribution is used, N_0, μ, and Λ can be obtained from Z_H, Z_{DR}, and K_{DP} by solving a system of three nonlinear equations. For real applications, there are various errors, including microphysics (MP; DSD, shape, orientation) modeling error, electromagnetic (EM) scattering modeling error, and radar measurement (Z_H, Z_{DR}, and K_{DP}) errors. These errors cause uncertainty and sometimes result in no solution in rain DSD retrievals from polarimetric radar data (PRD). If an additional constraint is introduced for the gamma distribution (e.g., EXP or C-G), the inverse problem becomes more complicated. Thus, a DSD retrieval framework based on the EMA was introduced. The EMA is based on the idea of optimization using forward operators. The parameters in the DSD model are refined step by step according to the difference of the radar parameters synthesized from the DSD against the measurements. When the difference is minimized, the DSD is optimally estimated. The measurement errors are taken into account in the EMA by normalizing the terms in the cost functions by the corresponding error terms ($\sigma_{Z_H}, \sigma_{Z_{DR}}$, and $\sigma_{K_{DP}}$). For EXP and C-G, the terms regarding K_{DP} can be removed from the optimization by increasing the corresponding error term $\sigma_{K_{DP}}$ to infinity. Then, only Z_H and Z_{DR} are required for the calculation of the DSD parameters. The formulas and details of the framework are described in the appendix. Using this framework, the impact of the exclusion of K_{DP} from the DSD retrieval was demonstrated by the sensitivity experiments described in sections 3 and 4.

The DSD data used in this study were collected by a two-dimensional video disdrometer (2DVD) located at Nanjing, China, in the summers of 2014 and 2015. The position of the 2DVD was indicated by the black dot shown in Fig. 1. Before collecting data, the 2DVD was calibrated by measuring metal balls with known size dropped into the orifice every year. The time resolution for the DSD integration was 1 min. Total number of the DSD samples used for the simulations in this study was 21 739. More details of the dataset can be found in Wen et al. (2016). With the DSD dataset, the μ–Λ relation for the summer precipitation in this region was derived using a method of sorting and averaging based on two parameters (SATP; Cao et al. 2008), resulting in

$$\mu = -0.017\,60\Lambda^2 + 0.9472\Lambda - 1.687. \tag{4}$$

To assess the performance of the DSD retrievals, simulated polarimetric data were calculated from the observed DSDs following Eqs. (1)–(3). The polarimetric measurements were simulated by adding Gaussian random errors into the synthetic polarimetric data. After estimating $N(D)$ from these simulations, the physical parameters (R, W, D_m, and N_t) were derived following the formulas in Zhang (2016). In calculating R, the statistical terminal velocity derived by Brandes et al. (2004a) was used. Because N_t data usually have a very large dynamic range, they were shown using the logarithmic scale in this study. The physical parameters calculated from the observed DSDs were treated as the truth for natural rain, and the retrievals were compared with them using four common parameters, namely, the correlation coefficient (CC), the fractional error (FE), the bias (BIAS), and the root-mean-square error (RMSE), which were calculated as follows:

$$\mathrm{CC} = \frac{\sum_{i=1}^{N}(V_{e,i} - \overline{V}_e)(V_{d,i} - \overline{V}_d)}{\sqrt{\sum_{i=1}^{N}(V_{e,i} - \overline{V}_e)^2 \sum_{i=1}^{N}(V_{d,i} - \overline{V}_d)^2}}, \tag{5}$$

$$\mathrm{FE} = \frac{\frac{1}{N}\sum_{i=1}^{N}|V_{e,i} - V_{d,i}|}{\overline{V}_d}, \tag{6}$$

$$\mathrm{BIAS} = \frac{1}{N}\sum_{i=1}^{N}(V_{e,i} - V_{d,i}), \tag{7}$$

$$\mathrm{RMSE} = \left[\frac{1}{N}\sum_{i=1}^{N}(V_{e,i} - V_{d,i})^2\right]^{1/2}, \tag{8}$$

where V_e is the one of the physical parameters (R, W, D_m, and N_t) estimated from the retrieved DSD, and

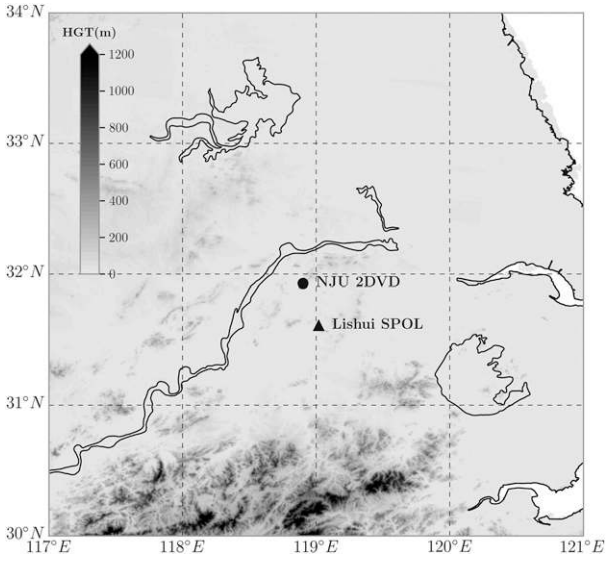

FIG. 1. The topography around Lishui S-Pol (black triangle) and NJU 2DVD (black dot). The elevation of the terrain is indicated as shading.

V_d is the truth calculated from the disdrometer data. The overbar indicates the mean value of the N samples.

3. The feasibility of the gamma distribution–based DSD retrieval

The gamma distribution has been widely used to characterize rain properties for several decades (Ulbrich 1983). Nevertheless, whether the gamma distribution can be directly used to retrieve the DSD from Z_H, Z_{DR}, and K_{DP} still remains to be proven. Two major sources of errors in the retrieval are the DSD model error and measurement error, which were analyzed as follows.

a. DSD model error effects

In the formulation of the DSD retrieval Eqs. (1)–(3), rain DSD is assumed to be gamma distributed so that the three DSD parameters (N_0, μ, and Λ) can be solved from the three radar variables (Z_H, Z_{DR}, and K_{DP}). In reality, rain DSD may not be exactly gamma distributed. There is a model representation error in the gamma distribution, which will in turn cause an error in DSDs retrieved from polarimetric measurements, which also contain errors. To study the DSD model effects, the EMA-based approach was used with simulated polarimetric radar data. Gamma DSD parameters were estimated from the Z_H, Z_{DR}, and K_{DP} simulated directly from the 2DVD data (see section 2). No measurement errors were included in the radar data, and the values of the error terms in the EMA were set to be very small, as explained in the appendix. Then, R, W, D_m, and N_t were calculated from the retrieved DSD for comparison with the corresponding observations (Fig. 2). The results based on the C-G and EXP are provided as references. Overall, the performance of the three-parameter GM was worse than that of the C-G. The deviations of retrieved R, W, and N_t from the truth were obvious, exhibiting generally larger RMSE, BIAS, and FE values than the C-G. The performance of D_m was better than the other three parameters but was still not satisfactory. Although the C-G was based on the gamma distribution, an extra constraint (the μ–Λ relation) made the estimated physical parameters more consistent with those from the observations. The RMSE, BIAS, and FE values were generally low and CC values were high. However, the performance of the EXP was much worse than that of the C-G, even though the EXP was also essentially the gamma distribution with $\mu = 0$. The values of RMSE, BIAS, and FE for the EXP were even greater than those for the three-parameter GM, suggesting that simply fixing $\mu = 0$ was a nonrealistic constraint. The differences between the physical parameter estimates (R, W, D_m, and N_t) based on the three-parameter GM and the values derived from the DSD observations were mainly caused by its model representation error. Note that, since R and W are close as the DSD moments, they reveal similar behaviors consistently in the comparative study. Thus, most of the results for R were not shown in the rest of the study for simplicity.

In studies of rain properties, the observed DSDs are usually fitted to the three-parameter GM. Here, the untruncated-moment method using the second, fourth, and sixth moments were adopted (Vivekanandan et al. 2004; Zhang 2016). The difference between the fitted DSDs and those retrieved from the radar variables clearly illustrated the errors caused by the different models. Comparisons of the physical parameters calculated from the fitted DSDs and those estimated from the retrieval are shown in Fig. 3. In this simulation, we also assumed that the scattering condition was known. If the natural DSDs exactly followed the assumed three-parameter GM, the retrieved DSDs based on the three-parameter GM would be exactly the same as the fitted ones. Nevertheless, there were significant differences between the physical parameters calculated from the fitted DSDs and those estimated from the retrieved DSDs based on the three-parameter GM, which validated the conclusion obtained from Fig. 2. DSD truncation is an important factor that needs to be considered when representing the natural DSD with the gamma distribution (Vivekanandan et al. 2004). As noted earlier, D_{max} is not easy to determine from polarimetric measurements, and therefore it is usually given an assumed fixed value (e.g., 8 mm) in the

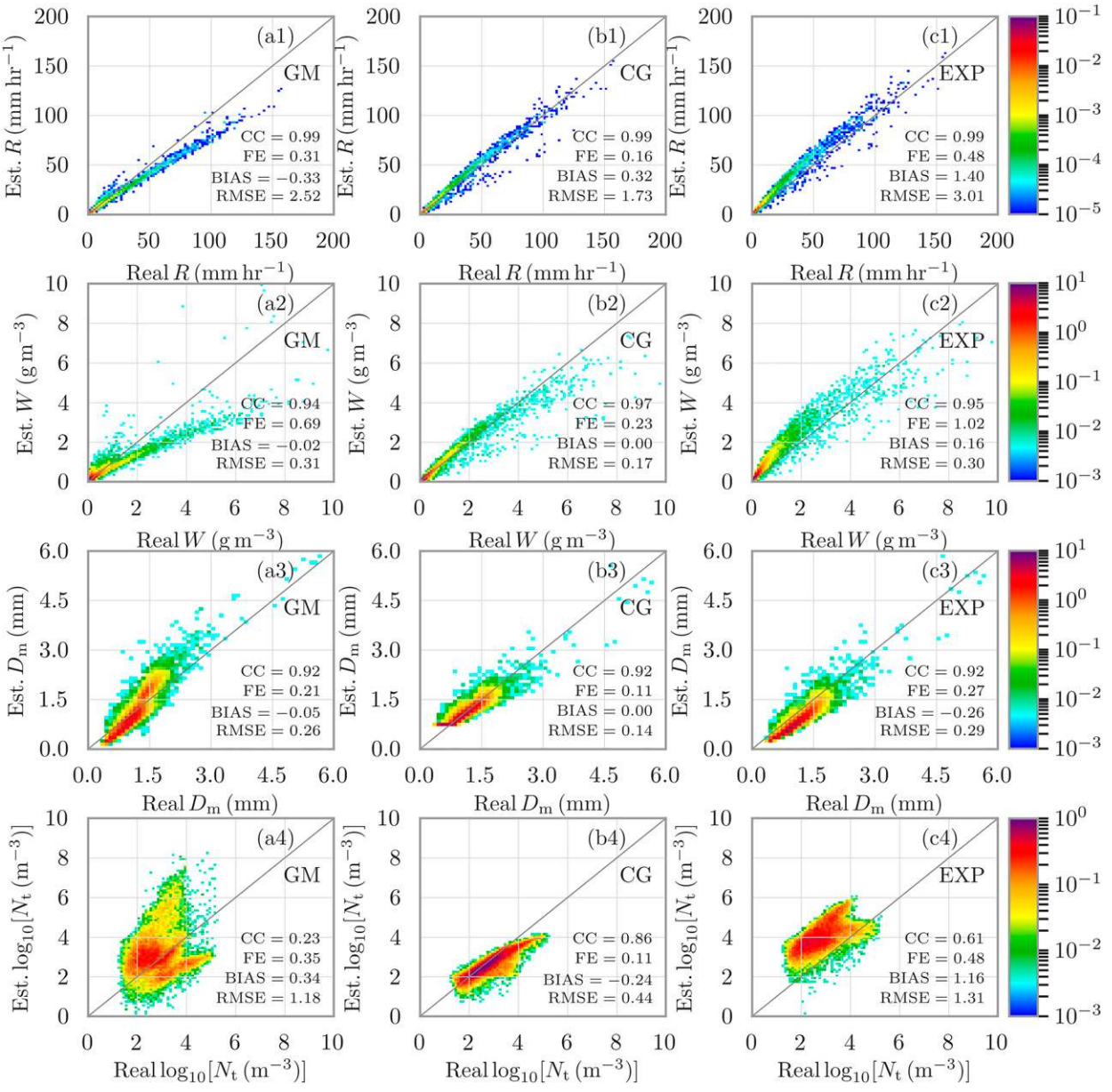

FIG. 2. Comparisons of (a1),(b1),(c1) R; (a2),(b2),(c2) W; (a3),(b3),(c3) D_m; and (a4),(b4),(c4) N_t calculated from the 2DVD observations against those from the retrieved DSDs. The shading means the two-dimensional probability density. The category sizes of R, W, D_m, and N_t are 2 mm h^{-1}, 0.1 g m^{-3}, 0.1 mm, and 0.1 log$_{10}$(m^{-3}), respectively. The DSDs were retrieved from the synthetic Z_H, Z_{DR}, and K_{DP} based on the three-parameter (a1)–(a4) GM, (b1)–(b4) C-G, and (c1)–(c4) EXP, respectively.

retrieval (Zhang et al. 2001), which is not true for the observed DSD. The inconsistency between the natural DSD and the gamma distribution may also be partially attributed to the microphysical processes of precipitation, for example, the evaporation, collision coalescence, and breakup processes (Kumjian and Ryzhkov 2010; Kumjian and Prat 2014). The size sorting process may cause the "long tail," suggesting an increase in the concentrations of larger raindrops and a decrease in the concentration of small raindrops (Cao and Zhang 2009). Furthermore, the polarimetric variables and the parameters of gamma distribution are not independent, which leads to an ill-posed retrieval problem using the three-parameter GM. As a result, the retrieved physical parameters are not consistent with the truth in Fig. 2.

As indicated by Figs. 2 and 3, the impact of the inconsistency between the natural DSD and the models weakened as extra constraints were used. In this study,

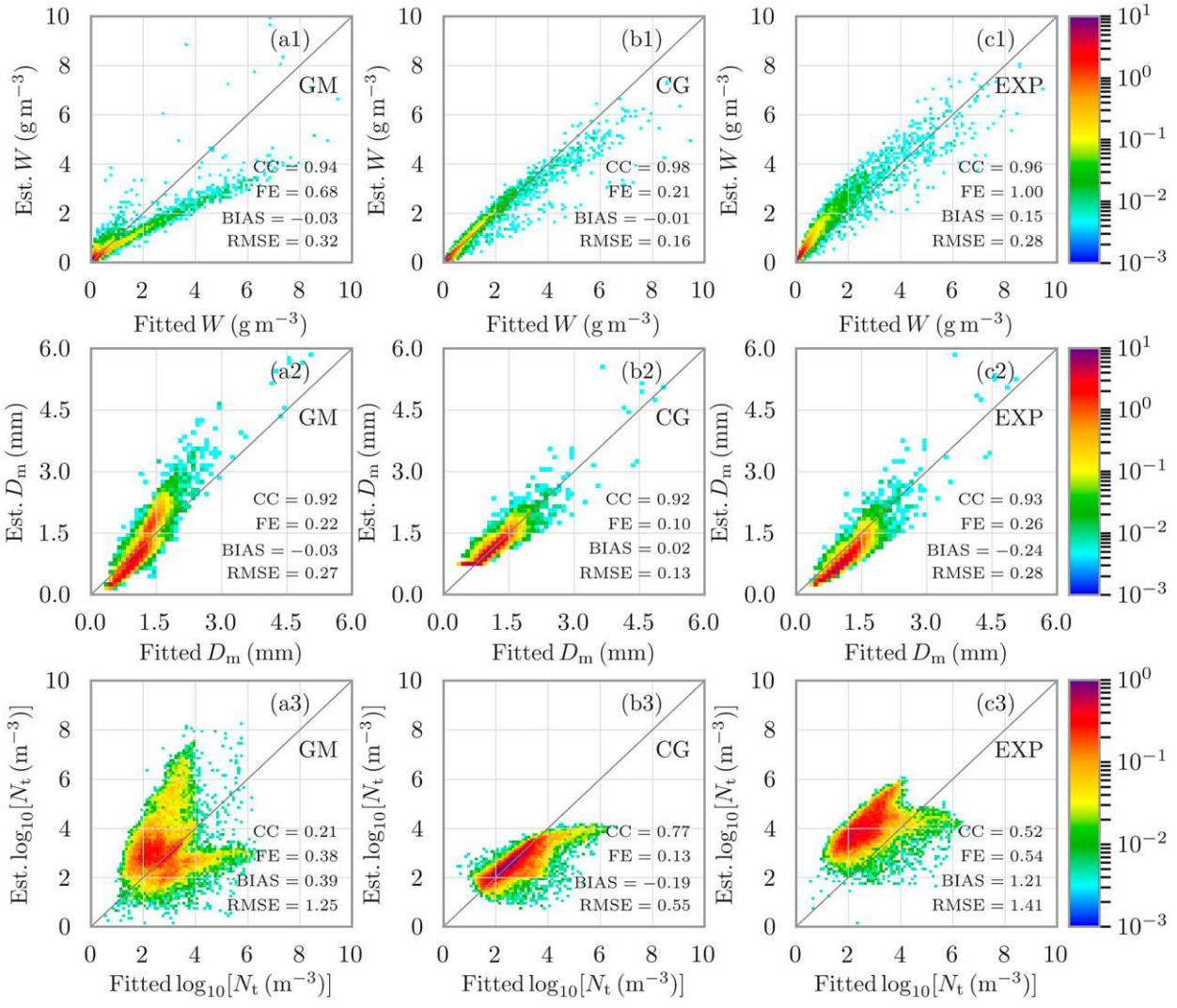

FIG. 3. As in Fig. 2, but for a comparison of the physical parameters calculated from fitted DSDs with those from the retrieved DSDs.

the μ–Λ relation used in C-G had better performance than the constraint of EXP ($\mu = 0$). Based on the C-G, better DSDs and corresponding rain parameters can be retrieved from the synthetic polarimetric variables. The μ–Λ relation can be considered to represent the physical property of natural rain and helps to reduce the uncertainties in DSD retrievals (Zhang et al. 2003).

b. *The impacts of simulated measurement errors*

Although polarimetric measurements provide valuable information regarding rain microphysical properties, measurement errors sometimes prevent their effective use and should be rigorously handled in DSD retrievals. To evaluate the impacts of these errors quantitatively, polarimetric measurements were simulated by adding Gaussian random errors to the calculated radar variables from a 2DVD dataset. In this analysis, the standard deviations of the simulated errors for Z_H, Z_{DR}, and K_{DP} were 1 and 0.2 dB and 0.3° km^{-1} respectively (Bringi and Chandrasekar 2001; Ryzhkov et al. 2003; Lee 2006). As such, the error terms in the EMA-based retrieval were assumed to be known, namely $\sigma_{Z_H} = 1$ dB, $\sigma_{Z_{DR}} = 0.2$ dB, and $\sigma_{K_{DP}} = 0.3°\,\text{km}^{-1}$. The physical parameters of rain calculated from retrieved DSDs based on the three-parameter GM, C-G, and EXP were compared with the truth, as shown in Fig. 4. The physical parameters were less accurate due to the measurement errors. Different DSD models had different levels of sensitivity to the measurement errors. Compared with the results of the C-G, the retrievals based on the three-parameter GM had fewer constraints, making them more sensitive to measurement

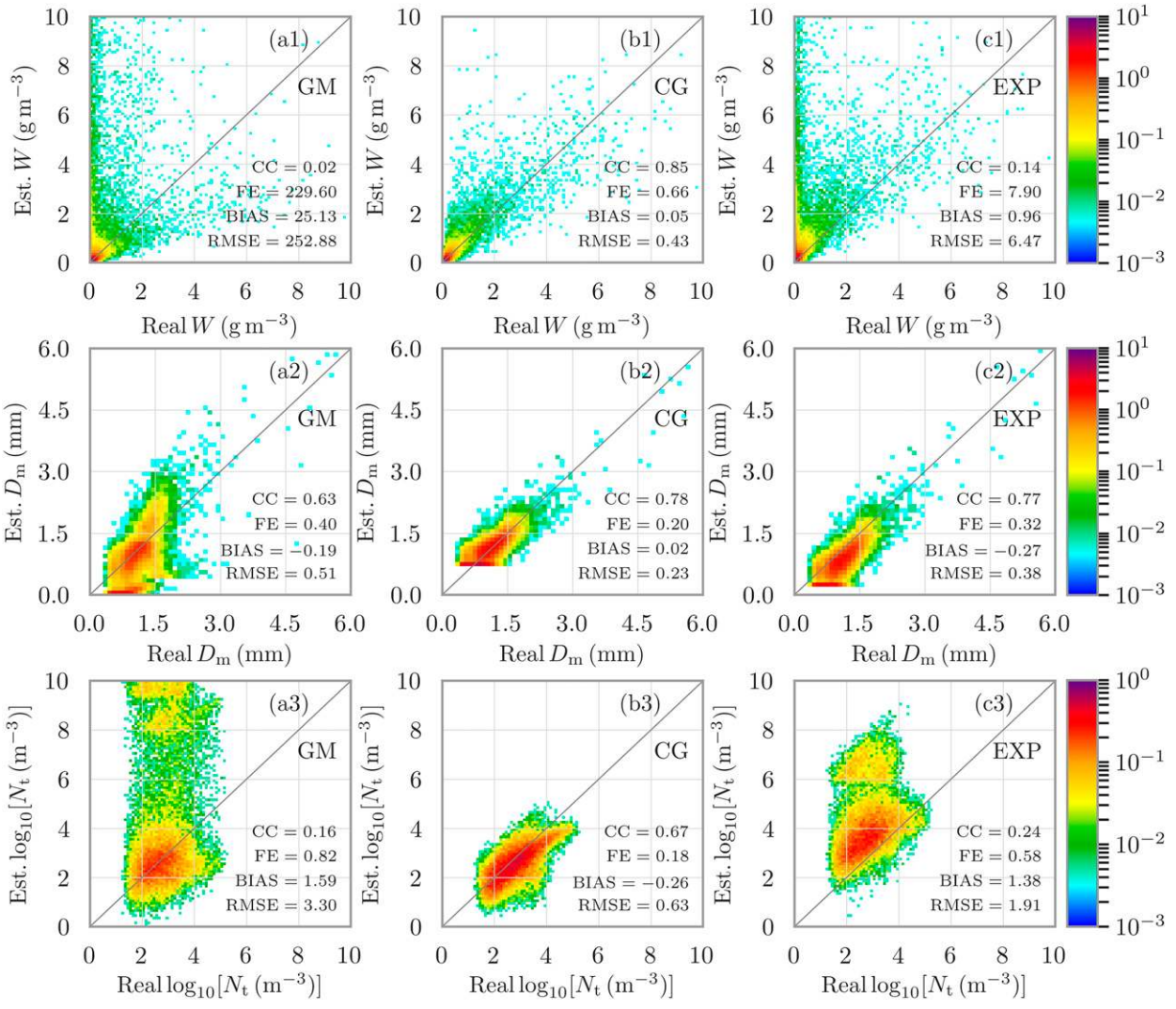

FIG. 4. As in Fig. 2, but with errors in the measurements ($\sigma_{Z_H} = 1$ dB, $\sigma_{Z_{DR}} = 0.2$ dB, and $\sigma_{K_{DP}} = 0.3°\,\text{km}^{-1}$).

errors. Thus, the results based on the three-parameter GM deteriorated significantly, with increased RMSE, FE, and BIAS, and a very low CC. The results of the C-G also indicated reduced accuracy in the physical parameters, although the overall performance was satisfactory. The impacts of the measurement errors were diminished by the constraint in the C-G. For the EXP, negative errors in Z_{DR} and K_{DP} also affected the estimates of the physical parameters, with greater errors than C-G. The R, W, and N_t estimates were positively biased, while D_m estimates were negatively biased.

It should be noted that no valid estimates can be obtained if Z_{DR} or K_{DP} values were negative in conventional retrieval using C-G or EXP (Seliga and Bringi 1976; Zhang et al. 2001). However, the EMA-based approach made it possible to obtain valid estimates under such conditions, which is the advantage of this kind of optimization-based retrieval.

c. *The feasibility of the three-parameter GM-based DSD retrieval*

Some conclusions can be drawn from the analyses in the preceding two subsections. Neither radar measurements nor the parameters of gamma distribution were completely independent for natural rain, which makes the retrieval using the three-parameter GM alone ill-conditioned. For natural rain, even without errors in the polarimetric measurements, the retrieved physical parameters based on the three-parameter GM showed significant deviations from the truth. They also showed large sensitivities to the measurement errors. The errors in the radar measurements may increase due to the contaminated

echoes or echoes with a lower radar signal-to-noise ratio (SNR). Under these circumstances, the results would become even worse than those in the simulations, indicating the importance of additional constraints in the gamma distribution.

4. The roles of K_{DP} in DSD retrieval

a. Comparison of retrievals with and without K_{DP}

From the quantitative studies in the previous section, we found that the C-G had advantages over the three-parameter GM and EXP when retrieving DSDs from Z_H, Z_{DR}, and K_{DP} measurements. Before the EMA-based or other optimization-based approaches were developed, DSDs were commonly retrieved from Z_H and Z_{DR} databased on the DSD models with 2 degrees of freedom, for example, C-G and EXP (Zhang et al. 2001; Brandes et al. 2004a). The K_{DP} is not a direct radar measurement but is obtained from the range derivative of Φ_{DP} (°) over multiple gates. The measurement errors of K_{DP} are not only from the random errors in Φ_{DP} measurements but also from the average of the physical variabilities of rain (Huang et al. 2017). Thus, the resolution volume of K_{DP} is different from Z_H and Z_{DR} (Zhang 2016), and many studies only use Z_H and Z_{DR} in DSD retrievals (Zhang et al. 2001, 2003; Zhang 2016). Even so, K_{DP} measurements still contain valuable information about rain (Gosset et al. 2010), and proper utilization of K_{DP} may potentially improve DSD retrievals. In the EMA-based approach, if the error term of K_{DP} is set to infinity, only Z_H and Z_{DR} measurements will play roles in the retrievals, which allows for a quantitative evaluation of how K_{DP} measurements affect the retrievals.

First, the intrinsic representatives of C-G and EXP for the natural rain were investigated when K_{DP} was not included. Similar to the simulation in section 3a, no measurement errors were added to the polarimetric data. The results are shown in Fig. 5. The K_{DP} values were calculated from the retrieved DSD and were compared with the synthetic K_{DP} from the 2DVD dataset, which was similar to the estimation of K_{DP} from Z_H and Z_{DR} based on their self-consistent relations (Vivekanandan et al. 2003; Huang et al. 2017). The high consistency between K_{DP} calculated from the retrieved DSD and the 2DVD dataset [Figs. 5a(1),b(1)] indicated that both C-G and EXP retained self-consistency among the polarimetric variables. If K_{DP} was excluded from the retrievals, negligible changes appeared in W and D_m according to the comparison between Fig. 5 and Figs. 2b and 2c. The results for N_t and R (not shown) were also similar and are not shown for simplicity. The similarity suggests that, due to the self-consistency of the polarimetric variables, K_{DP} provides little independent information if no error exists in the polarimetric data.

However, the measurement error effect cannot be underestimated. It is worth investigating how K_{DP} contributes to DSD retrieval when errors exist in radar measurements. Similar to the experiment described in section 3b, another retrieval experiment was conducted in which the K_{DP} measurements were not included. The evaluation of the physical parameters is shown in Fig. 6. According to the comparison between Fig. 6 and Figs. 4b and 4c, the errors in D_m and N_t did not significantly change when K_{DP} measurements were not used in the retrievals. However, the errors in W and R slightly increased for the C-G but decreased for the EXP, suggesting different roles of the K_{DP} measurements (see RMSE, FE, BIAS, and CC).

The integrated effects of K_{DP} may depend on the DSD model. For EXP, if the radar echo intensity is moderate (e.g., Z_H around 40 dBZ), the negative K_{DP} caused by the measurement error may have two different effects, as shown in Table 1. With no Z_{DR} errors (0 dB in Table 1), the negative K_{DP} tended to result in a lower D_m and larger R/W. However, with a large negative error in the Z_{DR} measurement (e.g., −0.55 dB), the negative K_{DP} may result in a very large Λ and large N_0 (note $\mu = 0$ for EXP), which represents a high concentration of very small raindrops, resulting in extreme positive biases in the estimated R and W and a negative bias in D_m. In such a case, the retrieval without K_{DP} measurements was better than that with K_{DP} measurements included.

For the C-G, the above situation did not cause severe biases because the concentration of the small drops was suppressed by the positive μ required by the μ–Λ relation, which mitigated the impacts of measurement errors. As shown by the comparison of Figs. 4 and 6, the incorporation of K_{DP} measurements enhanced the accuracy of the DSD retrieval, and hence the accuracy of the physical parameters W and R. When measurement errors exist, less information is provided by Z_H and Z_{DR}. Under such condition, the incorporation of K_{DP} made a positive contribution due to self-consistency of polarimetric variables. Because the C-G has two parameters that need to be determined, the measurement errors generally cannot be removed or canceled if only Z_H and Z_{DR} are used in the DSD retrieval. By using the EMA-based approach, the DSD was optimized under the statistical constraint of the C-G, with the consideration of errors in Z_H, Z_{DR}, and K_{DP}. The constraint provided by the μ–Λ relation reflects the physical property of rain (Zhang et al. 2003). Thus, the optimized DSDs from Z_H, Z_{DR}, and K_{DP}

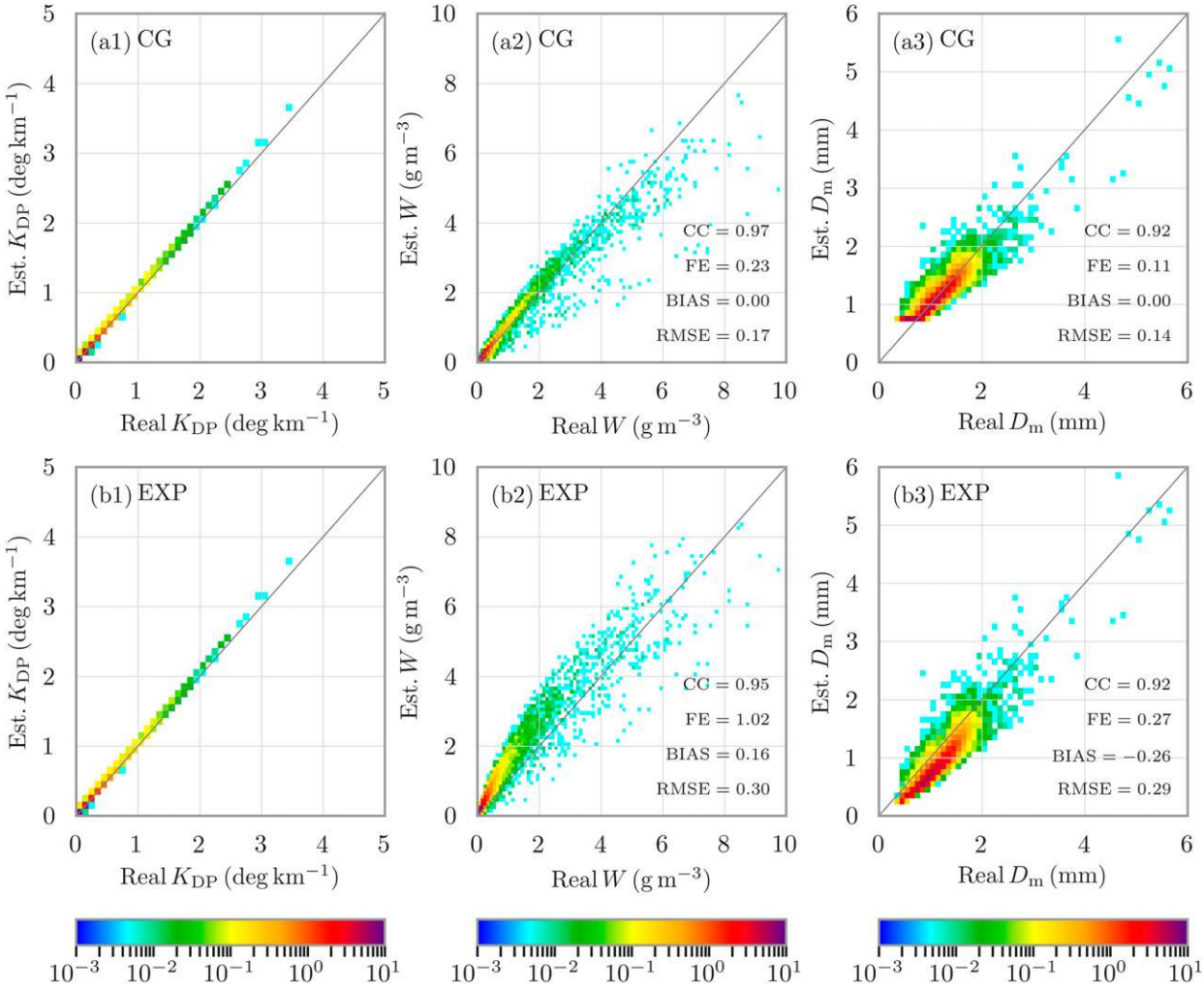

FIG. 5. Comparisons of (a1),(b1) K_{DP}; (a2),(b2) W; and (a3),(b3) D_m calculated from the retrieved DSDs against those from the 2DVD observations. The shading means the two-dimensional probability density. The category sizes of K_{DP}, W, and D_m are 0.1° km^{-1}, 0.1 g m^{-3}, and 0.1 mm. The DSDs are retrieved from the synthetic Z_H and Z_{DR} based on the (a1)–(a3) C-G distribution and (b1)–(b3) EXP, respectively.

were more realistic and less affected by the measurement errors.

b. *Quantitative evaluation of the impact of K_{DP} on the retrieval*

The impact of incorporating K_{DP} in the retrieval was shown in the previous subsection. The C-G had an advantage over the EXP when we attempted to obtain the most accurate DSD estimates by combining all the useful information of the polarimetric variables. In the earlier experiments, the standard deviation of the K_{DP} errors was assumed to be equal to 0.3° km^{-1}. However, in recent years, novel approaches have been proposed for more accurate K_{DP} estimates, including an approach based on linear programming (Giangrande et al. 2013), the hybrid method (Huang et al. 2017), and the variational approach (Maesaka et al. 2012; Huang et al. 2018). The errors in K_{DP} can be reduced by incorporating physical constraints or by an optimization using all of the useful information provided by polarimetric radars. On the other hand, when a radar echo is contaminated by nonmeteorological scatterers or when the radar SNR decreases, the backscattering phase or random errors in Φ_{DP} can increase significantly. Unfortunately, these can cause larger errors in K_{DP} (Bringi and Chandrasekar 2001, chapter 6). Moreover, K_{DP} on a radar gate is calculated based on a series of sequential Φ_{DP} data at its neighboring range gates. Large spatial variabilities in these range gates will cause more errors and uncertainties in the K_{DP} estimates.

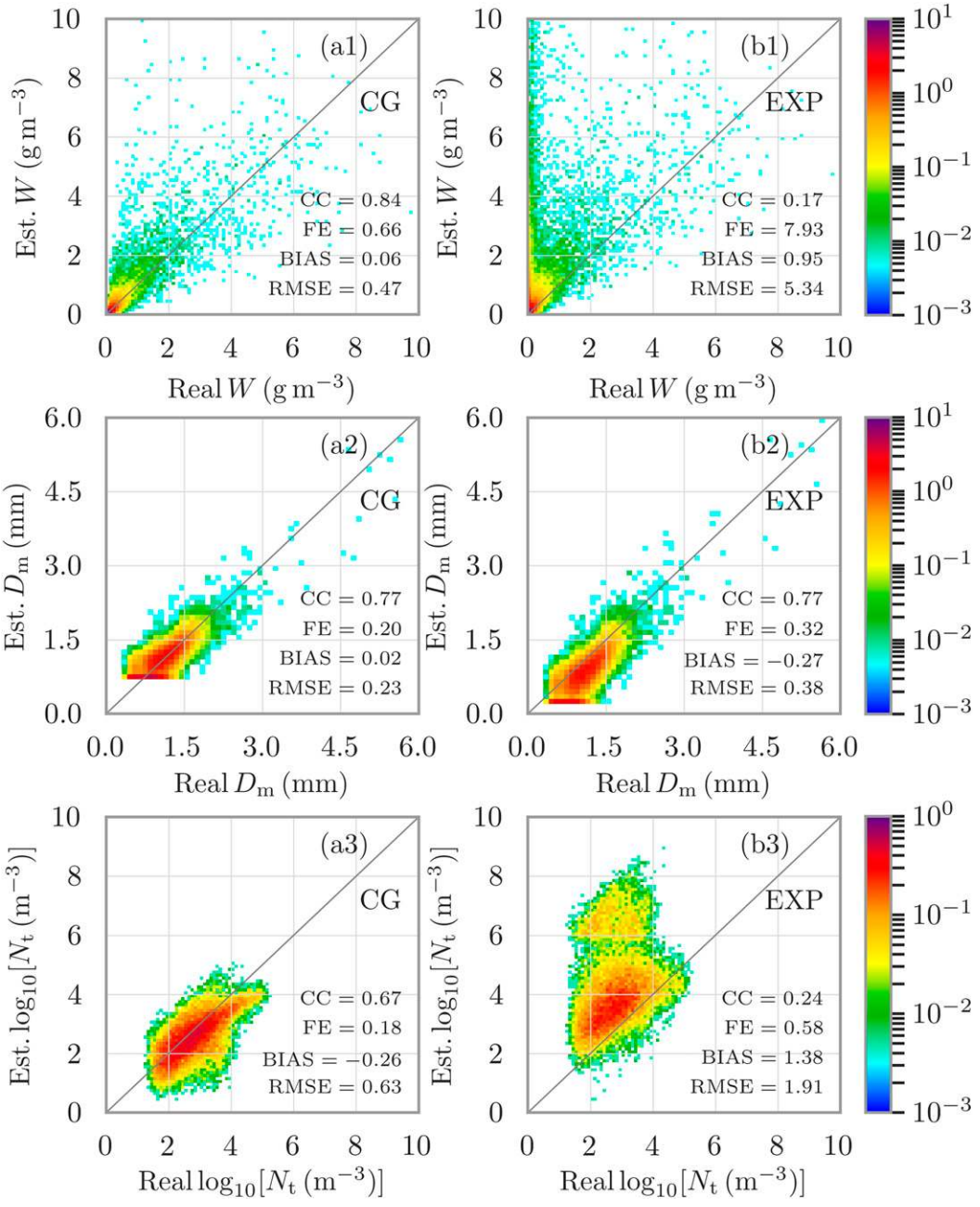

FIG. 6. As in Fig. 4, but for retrievals using Z_H and Z_{DR} measurements based on the (a1)–(a3) C-G distribution and (b1)–(b3) EXP.

To study quantitatively how K_{DP} measurements with different error levels can affect the accuracy of DSD retrieval, six groups of comparative experiments were designed. All of these sensitivity experiments used the same group of simulated Z_H and Z_{DR} measurements with $\sigma_{Z_H} = 1$ dB and $\sigma_{Z_{DR}} = 0.2$ dB (see section 3b for the simulation of radar measurements). In the control experiment, the K_{DP} measurements were not used in the retrievals. In the other five groups of sensitivity experiments, we used simulated K_{DP} measurements with different levels of Gaussian random error and standard deviations ranging from 0.1° to 0.5° km^{-1}, with a 0.1° km^{-1} interval. DSDs were then retrieved from the simulated radar measurements using the EMA-based approach. The error terms in the EMA were assumed to be known and correctly used in all sensitivity measurements. Only the C-G was used as the model for DSD retrieval because the EXP and the

TABLE 1. The performance of the retrieved physical parameters (R, W, and D_m), with two different levels of errors included. The retrieval was based on the polarimetric data calculated from an observed DSD (Z_H = 39.962 dBZ, Z_{DR} = 0.597 dB, K_{DP} = 0.245° km^{-1}).

			R (mm h^{-1})	W (g m^{-3})	D_m (mm)
		Truth	24.01	1.43	1.3
ε_{Z_H} = 0.0	With K_{DP}	C-G	24.82	1.46	1.31
$\varepsilon_{Z_{DR}}$ = 0.0		EXP	30.45	2.13	1.07
$\varepsilon_{K_{DP}}$ = −0.6	Without K_{DP}	C-G	26.19	1.55	1.3
		EXP	32.21	2.27	1.06
ε_{Z_H} = 0.0	With K_{DP}	C-G	118.25	11.25	0.71
$\varepsilon_{Z_{DR}}$ = −0.55		EXP	1040.75	344.95	0.2
$\varepsilon_{K_{DP}}$ = −0.6	Without K_{DP}	C-G	124.22	11.81	0.71
		EXP	281.2	47.74	0.39

three-parameter GM exhibit clear shortcomings in the DSD retrieval due to the lack of physical constraints.

The dependence of the retrieval accuracy on K_{DP} errors was then demonstrated with respect to the echo intensity (Z_H). As shown in Fig. 7, the synthetic Z_H from the DSD was separated into nine bins ranging from 12 to 48 dBZ with 4-dB intervals, and the CC, BIAS, FE, and RMSE of the physical parameters were calculated within each Z_H bin. The results demonstrated that there was no significant change for D_m when the measurement errors in the K_{DP} changed from 0.1° to 0.5° km^{-1} or even when K_{DP} measurements were not used in the retrieval. For W, N_t, and R, the accuracy of the retrieval changed when the errors in the K_{DP} measurements changed. This effect was not significant when the echo intensity $Z_H < 35$ dBZ, while the advantage of using more accurate K_{DP} measurements was clear when $Z_H > 35$ dBZ. Note that the threshold 35 dBZ was also adopted by Bringi et al. (2002) to determine whether K_{DP} should be used for DSD retrieval. The CC values increased and the RMSE, FE, and BIAS decreased when the errors in the K_{DP} measurements changed, indicating more accurate physical parameters and hence a more accurate DSD. This effect intensified as Z_H increased. Even when including K_{DP} measurements with relatively large errors ($\sigma_{K_{DP}} = 0.5°$ km^{-1}), the W, N_t, and R estimates were still more accurate than those estimated from the retrieval using only Z_H and Z_{DR} measurements. Note that N_t was in logarithmic scale. Thus, only the increase in CC was significant.

To investigate the underlying reason for this, the synthetic polarimetric variables calculated from the retrieved DSDs were compared with those calculated from the observed DSD data. Only the results for $\sigma_{K_{DP}} = 0.1°$ and 0.3° km^{-1} as well as those without K_{DP} are shown in Fig. 8. The comparisons between the estimated and the synthetic polarimetric variables indicate how much error was removed and how much propagated to the estimates. When the DSD was retrieved from two measurements (Z_H and Z_{DR}), most errors except the negative Z_{DR} could not be removed because there was no additional information. As a consequence, the errors in the estimated K_{DP} shown in Fig. 8a(3) were relatively large compared with those in Figs. 8b(3) and 8c(3). When K_{DP} was used, the errors in the three measurements could be partially canceled through the optimization because of the additional constraint in C-G. In the EMA-based retrieval, the error terms in the cost function acted as weightings or as a quality index for the measurements. When the errors in the K_{DP} measurements were reduced, K_{DP} contributed more to the estimation, especially when the echo intensity was severe (relatively large Z_H; see Fig. 7 and Fig. 8). Because Z_H was recorded using the decibel scale, the errors in Z_H had a large impact on the estimation of W, N_t, and R when Z_H was relatively large. Under such conditions, more useful information in K_{DP} contributed to the estimates since the effect of the errors in K_{DP} is linear. When $\sigma_{K_{DP}}$ decreased, more accurate information in K_{DP} resulted in more accurate estimation of W, N_t, and R (Figs. 7a and 7c). In the meantime, fewer Z_H errors propagated to the estimates, and Z_H estimates would become more accurate when $Z_H > 35$ dBZ [Figs. 8a(1)–c(1)]. However, Z_{DR} estimates barely changed even when very accurate K_{DP} measurements were used in the retrieval [Figs. 8a(2)–c(2)], corresponding to quasi invariability in the performance of the D_m estimates [Figs. 7b(1)–b(4)].

c. *Effects of the inaccurate characterization of the K_{DP} error properties*

As stated earlier, the advantage of the EMA-based retrievals was that all the available measurements were used according to their reliabilities, as determined by their error properties (error terms). Thus, accurate retrievals require relatively accurate characterization of the measurement errors. However, the K_{DP} errors are not easy to estimate quantitatively because they are derived not only from the errors in Φ_{DP} measurements but also from the uncertainty in the spatial variabilities

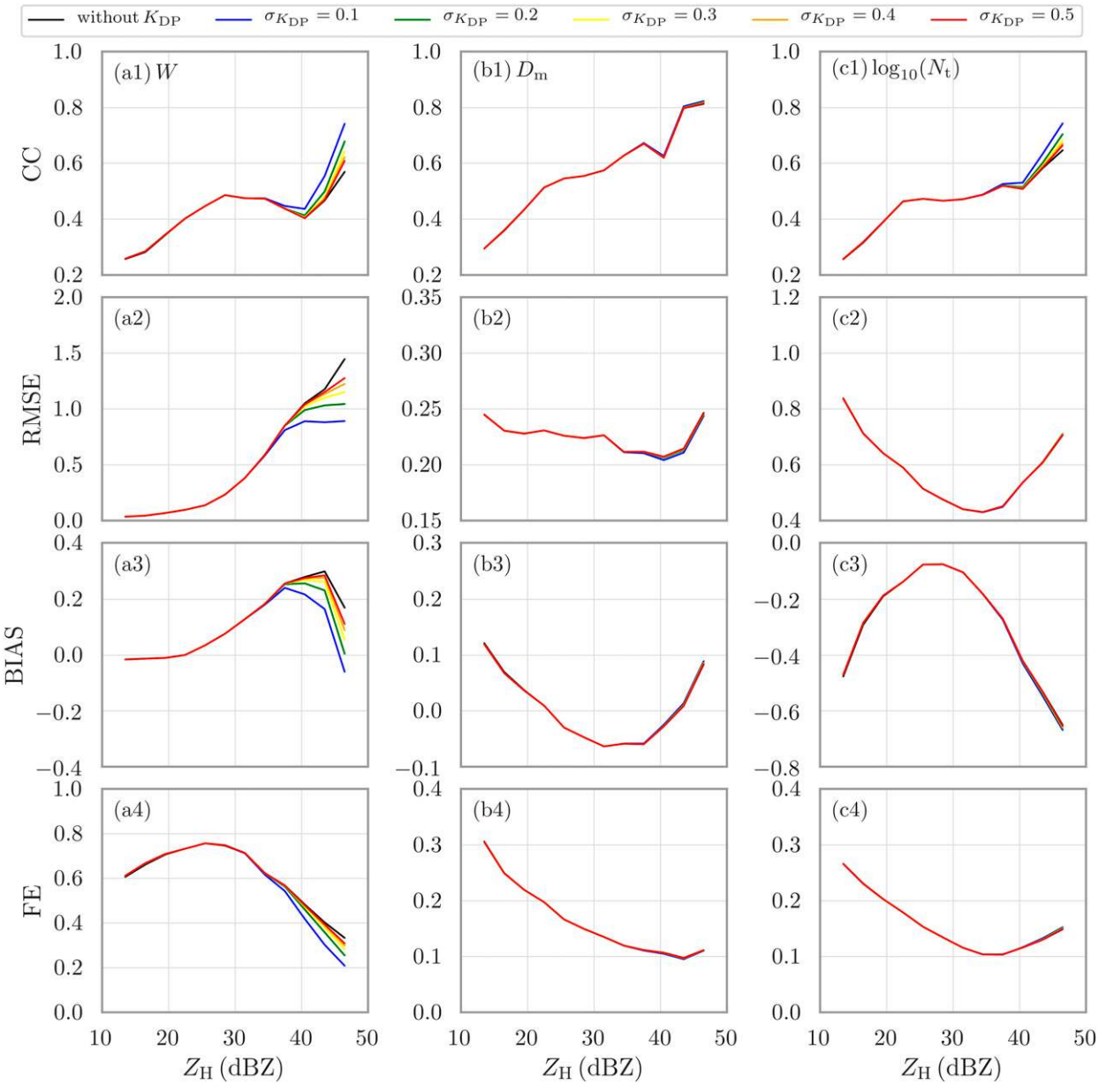

FIG. 7. Comparisons of (a1),(b1),(c1) CC, (a2),(b2),(c2) RMSE, (a3),(b3),(c3) BIAS, and (a4),(b4),(c4) FE corresponding to (a1)–(a4) W, (b1)–(b4) D_m, and (c1)–(c4) N_t calculated from the retrieved DSDs without K_{DP} measurements or with K_{DP} measurements including different random errors.

of rain properties. We next investigated how the performance of the retrieval changed when inaccurate K_{DP} error terms were used in the retrieval.

The following experiments were designed based on the earlier ones. Simulated radar measurements were obtained by adding Gaussian simulated errors to the synthetic polarimetric data ($\sigma_{Z_H} = 1$ dB, $\sigma_{Z_{DR}} = 0.2$ dB, $\sigma_{K_{DP}} = 0.3° \text{ km}^{-1}$). Unlike the previous experiments, the error properties of the K_{DP} measurements were assumed to be not well known. As listed in Table 2, the error terms ($\sigma_{K_{DP}}$) used in the EMA in the different experiments were 0.1°, 0.2°, 0.3°, 0.4°, and 0.5° km^{-1}. A retrieval with the accurate $\sigma_{K_{DP}}$ (0.3° km^{-1}) was used as a control experiment. From the RMSE, BIAS, FE, and CC of the physical parameters for each experiment, we found that the physical parameters became less accurate if inaccurate $\sigma_{K_{DP}}$ values were used. Among the four physical parameters, D_m was the least affected. The useful information in the K_{DP} measurements was insufficiently used if the overestimated $\sigma_{K_{DP}}$ was used in

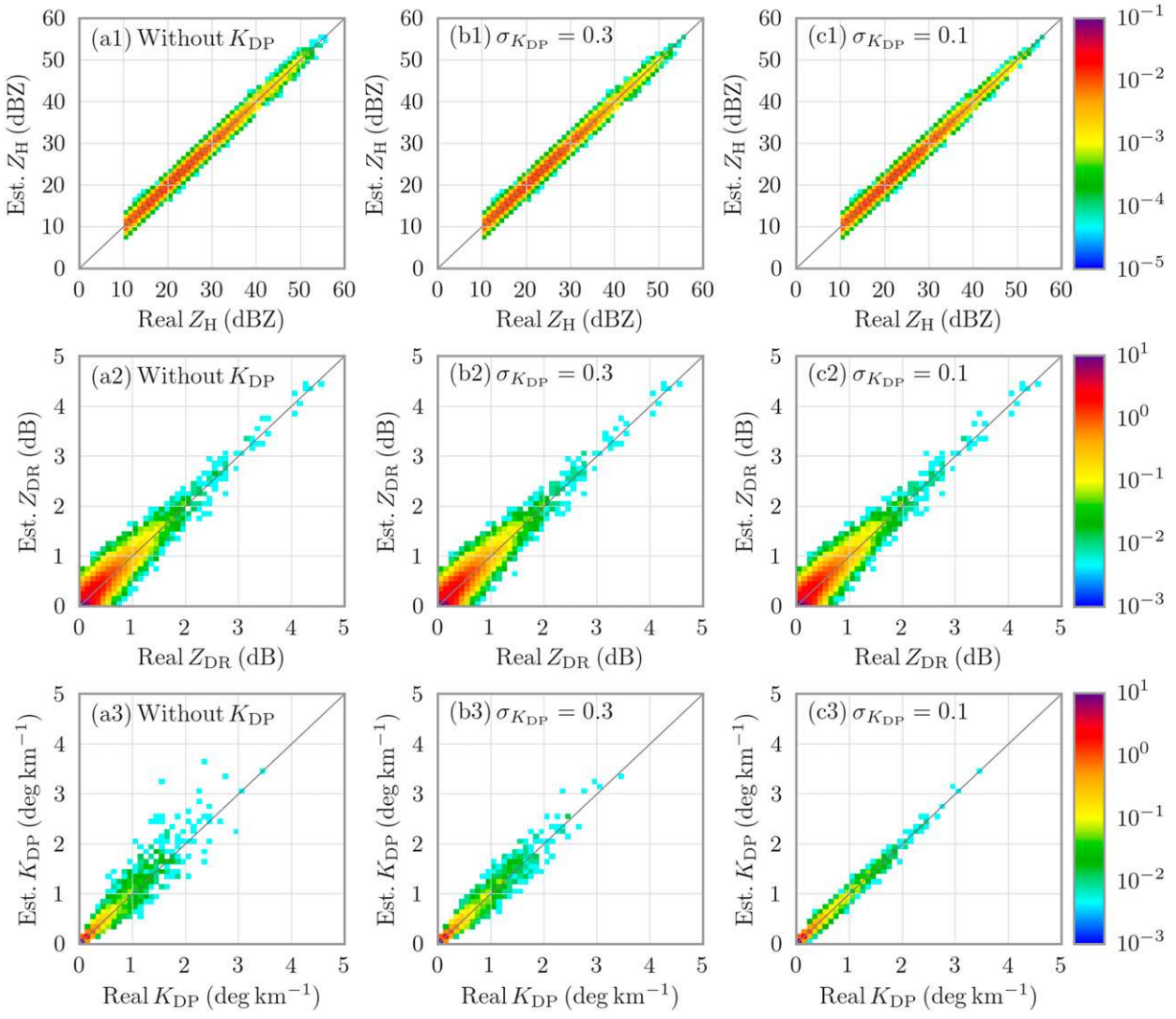

FIG. 8. Comparisons of synthetic (a1),(b1),(c1) Z_H, (a2),(b2),(c2) Z_{DR}, and (a3),(b3),(c3) K_{DP} from the retrieved DSDs against those from the 2DVD data. The shading means the two-dimensional probability density. The category sizes of Z_H, Z_{DR}, K_{DP}, R, and D_m are 1 dB, 0.1 dB, and 0.1° km^{-1}. (a1)–(a3) The results from the retrievals only using Z_H and Z_{DR} measurements. (b1)–(b3),(c1)–(c3) The results from the retrievals including measurements of different K_{DP} accuracy ($\sigma_{K_{DP}} = 0.3°\,\text{km}^{-1}$ and $\sigma_{K_{DP}} = 0.1°\,\text{km}^{-1}$, respectively).

the EMA. On the other hand, if a $\sigma_{K_{DP}}$ lower than the real error was used, the measurement errors in K_{DP} tended to propagate into the DSDs and the corresponding physical parameters. The retrievals under both situations were less accurate than that obtained when using an accurate $\sigma_{K_{DP}}$ The results from the experiments using overestimated $\sigma_{K_{DP}}$ values (0.4 or 0.5) were generally better than those obtained using underestimated $\sigma_{K_{DP}}$ values (0.1 or 0.2). This is probably because even when the information in K_{DP} measurements was underutilized, better results than those without K_{DP} measurements could still be obtained. However, by using underestimated $\sigma_{K_{DP}}$ values, the K_{DP} measurements were overly weighted. The useful information in Z_H and Z_{DR} measurements was lost and the K_{DP} errors overly propagated into the retrieval results. For example, even D_m can deteriorate when $\sigma_{K_{DP}} = 0.1°\,\text{km}^{-1}$ is used improperly. Therefore, when it is difficult to determine the errors in K_{DP} measurements, it is better not to use a relatively small $\sigma_{K_{DP}}$.

5. DSD retrieval in a real event

In the above study, simulation experiments based on observed DSD data were used to demonstrate the feasibility of directly retrieving the DSDs from polarimetric measurements based on the three-parameter GM and that including K_{DP} measurements with accurate error

TABLE 2. The performance of the estimated physical parameters (R, W, D_m, and N_t) for rain with different $\sigma_{K_{DP}}$ used in the error minimization analysis (EMA)-based retrieval.

$\sigma_{K_{DP}}$ (° km^{-1})		0.1	0.2	0.3	0.4	0.5
R (mm h^{-1})	CC	0.876	0.924	0.93	0.928	0.927
	FE	0.517	0.491	0.49	0.491	0.491
	RMSE	7.655	5.643	5.423	5.511	5.616
	BIAS	1.135	0.875	0.859	0.875	0.89
W (g m^{-3})	CC	0.778	0.839	0.846	0.843	0.842
	FE	0.689	0.659	0.657	0.658	0.658
	RMSE	0.57	0.445	0.431	0.438	0.443
	BIAS	0.07	0.051	0.05	0.051	0.052
D_m (mm)	CC	0.773	0.775	0.775	0.775	0.775
	FE	0.199	0.198	0.198	0.198	0.198
	RMSE	0.231	0.23	0.23	0.23	0.23
	BIAS	0.019	0.02	0.02	0.02	0.02
$\log_{10}[N_t$ (m^{-3})]	CC	0.664	0.666	0.667	0.666	0.667
	FE	0.18	0.18	0.18	0.18	0.18
	RMSE	0.635	0.633	0.632	0.632	0.632
	BIAS	−0.253	−0.255	−0.255	−0.255	−0.255

properties in the EMA-based retrieval led to more accurate DSDs and physical parameter estimates. Their performance will be investigated using real radar observations in the current section.

An S-band polarimetric radar called the Lishui radar (black triangle in Fig. 1) is located about 37 km to the southeast of the 2DVD. The radar was calibrated with a hollow metal sphere in June 2014, which ensured the accuracy of the radar reflectivity measurements. The Z_{DR} was calibrated by monitoring the Z_{DR} variations of the drizzle echo. The echoes with a correlation coefficient (ρ_{hv}) less than 0.8 were considered to be potentially contaminated by clutter or other nonmeteorological scatterers and were removed. The adaptive least squares fitting method similar to that adopted by WSR-88D was used to calculate K_{DP} (Huang et al. 2017); K_{DP} at each gate was obtained from the least squares fitting of Φ_{DP} within a specific fitting window. If the corrected Z_H is above (below) 40 dBZ, the length of the adaptive fitting window was set to 2.5 (9) km. On 12 and 3–4 July 2014, two precipitation systems passed over both the Lishui radar and the 2DVD. DSDs and physical parameters (R, W, D_m, and N_t) were retrieved from the radar measurements. The radar-derived parameters were quantitatively compared with the 2DVD observations to show the performance of different retrieving models.

The precipitation event on 12 July 2014 lasted for about 9 h. Figure 9 shows the plan position indicator (PPI) images of the radar scan at 0.5° elevation at 0640 UTC. The weather system produced both stratiform and convective precipitation. The Z_{DR} values were generally lower in the stratiform regions than in the convective regions, with substantial variation in the convective regions, indicating vastly different microphysical properties. The black lines in Fig. 10 show the synthetic polarimetric measurements generated from the 2DVD observations, while the red dots show the polarimetric radar measurements at 0.5° elevation above the 2DVD site for comparison. The rain DSDs sampled by the 2DVD contained both stratiform and convective precipitation. The vertical distance between the center of the radar volume and the 2DVD site was about 400 m. The radar measurements had a lower time resolution (about 7 min) than the 2DVD (1 min). Additional uncertainty in the comparison was led by different sampling volumes of these two different instruments as well as the evolution of hydrometeor microphysical properties while falling from the radar volume to the 2DVD site. Although sometimes no radar measurement was available while the 2DVD observed rain, overall the radar measurements corresponded well with the synthetic radar measurements calculated from the 2DVD-observed DSDs. Although the radar data were quality controlled, there were some negative Z_{DR} and K_{DP} measurements due to random errors and estimation errors, which may have affected the quality of the DSD retrieval.

Figure 11 shows the comparison of the retrieved physical parameters using four different approaches against the observations during the precipitation event on 12 July 2014. The green circles show the EMA-based retrieval using the three-parameter GM, the black triangles show the conventional retrieval using EXP, and the blue squares and the red dots show the results of the EMA-based retrieval using C-G with and without K_{DP} measurements respectively. The quantitative comparison between radar-derived rain physical parameters and

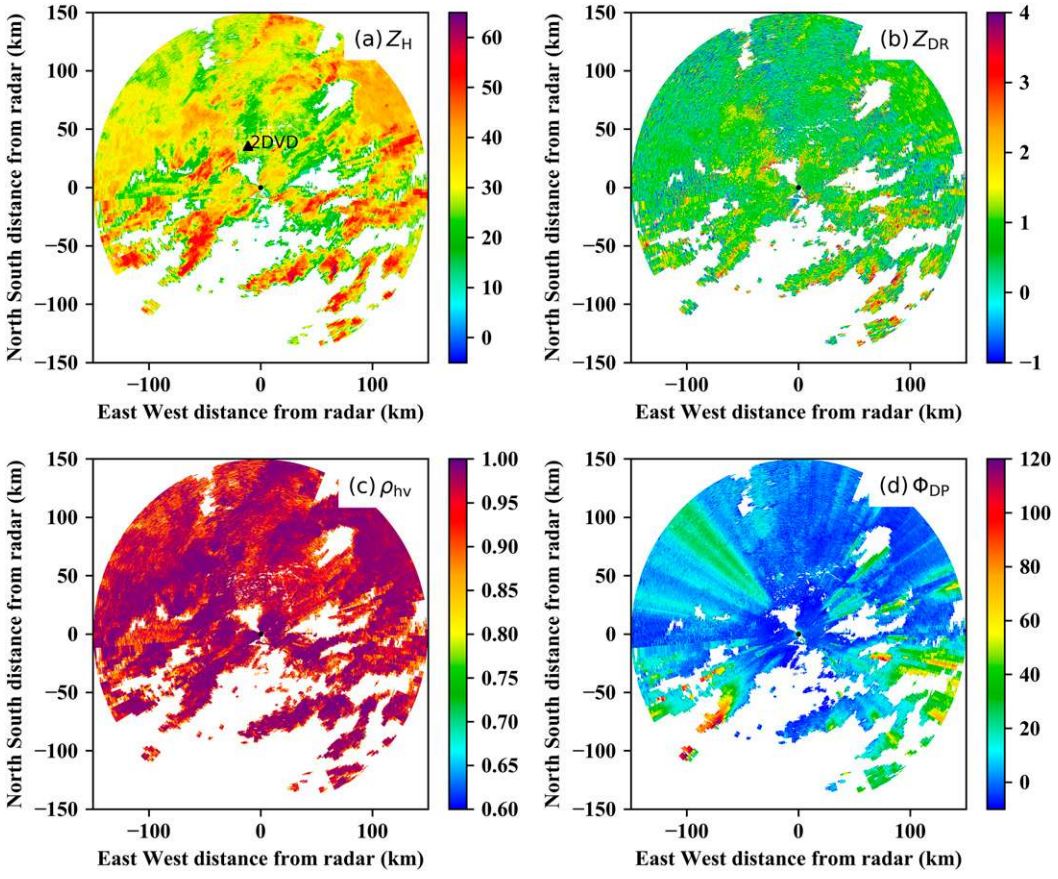

FIG. 9. Plan position indicator (PPI) images at 0.5° elevation for (a) Z_H, (b) Z_{DR}, (c) ρ_{hv}, and (d) Φ_{DP} from the Lishui radar at 0640 UTC 12 Jul 2017.

2DVD observations were show in Table 3. For R and W estimates, differences mainly existed when Z_H measurements were large (>45 dBZ; Fig. 11). When K_{DP} measurements were not used, the R and W estimates of EMA-based retrieval using C-G showed obvious overestimation, corresponding to the large RMSE and BIAS values. This overestimation also existed in the results of the conventional retrieval using EXP. When the K_{DP} measurements were used in the retrieval (denoted with blue squares), the results of EMA-based retrieval using C-G were more consistent with the 2DVD observations and the overestimations in R and W were diminished. The results of the above three approaches were not significantly different when the echo intensity was lower ($Z_H < 45$ dBZ; Fig. 11). However, the R and W estimates using three-parameter GM showed larger errors. The corresponding CC values were low, and the errors (FE and RMSE values) were high. In the D_m estimates, the results from EMA-based retrieval using C-G with and without K_{DP} measurements showed comparable accuracy, which was cross verified with the conclusions from section 4. Even though the CC values corresponding to these two kinds of estimates were not high, the low errors (FE, RMSE, and BIAS values) showed generally good consistency with the observation. For the D_m values, no valid values were obtained by the conventional retrieval using EXP when Z_{DR} measurements were negative. In addition, because the constraint in EXP ($\mu = 0$) was not completely suitable for the geographical region in this research, the D_m estimates from EXP showed lower accuracy than those from EMA-based retrieval using C-G. The retrieval using the three-parameter GM showed the lowest CC values and largest errors (FE, RMSE, and BIAS values). The estimates of N_t were the worst among the four physical parameters. This is mainly because N_t is the zeroth moment of DSDs, which is quite different from the moment orders of radar reflectivity (~sixth moment; Brandes et al. 2004a). This result is also consistent with the results shown in Figs. 4 and 6. The N_t estimates from the EMA-based retrieval using C-G with and without K_{DP} measurements showed comparable accuracy, while EXP-based retrieval showed lower accuracy. Then the N_t estimates from EMA-based retrieval using the three-parameter

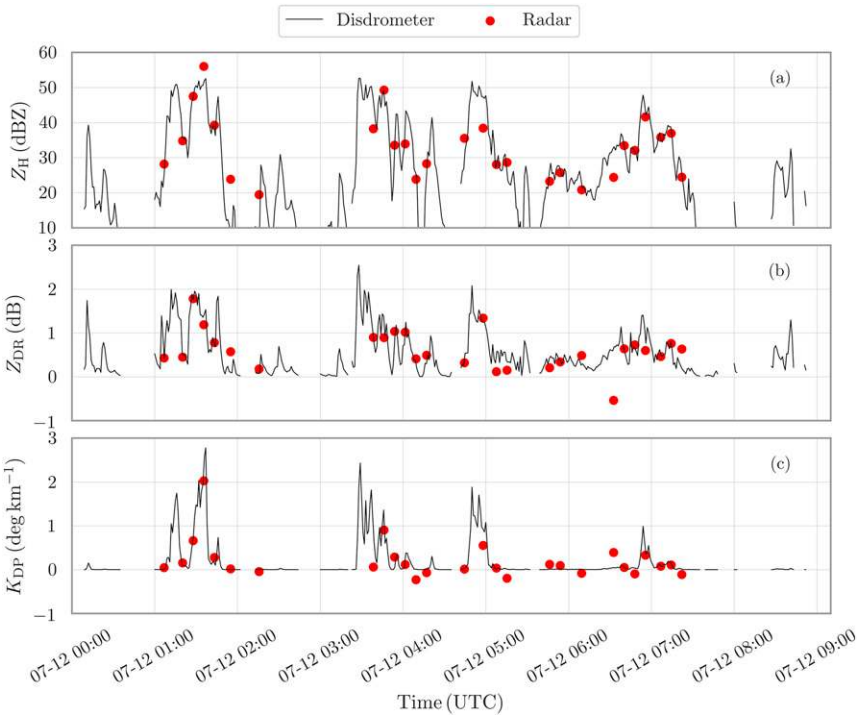

FIG. 10. Comparisons of radar measurements (a) Z_H, (b) Z_{DR}, and (c) K_{DP} denoted with red dots vs those calculated from the 2DVD data (black lines).

GM showed nearly no correlation with the observations (CC $\sim$ 0). The errors (FE, RMSE, and BIAS values) were also very large when compared with the results of the other methods.

The statistical comparison for another precipitation event that happened on 3–4 July 2014 was also shown in Table 3. In this event, the performance of radar-derived estimates (at 0.5° elevation) from the four approaches was similar to that in the event on 12 July 2014. The estimates from the EMA-based retrieval using the three-parameter GM also showed very large differences from the observations, which confirmed the conclusions from the simulation experiments. The conventional retrieval using EXP showed much better performance than the three-parameter GM especially for R, W, and D_m. For the EMA-based retrieval using C-G, slight improvements in R and W (decrease in The RMSE and BIAS) were found if the K_{DP} measurements were included, which was also consistent with the results shown in Fig. 7.

6. Conclusions and discussion

Estimating DSD parameters from polarimetric radar data facilitates precipitation microphysics research. It is important to know the error characteristics of the retrieval when using different methods. The three-parameter GM, C-G, and EXP are the three commonly used models for representing rain DSD retrieval. In this study, a general EMA-based approach was used to estimate DSDs based on these models. The performance of the DSD retrievals was investigated through simulation experiments and with real radar data.

First, the feasibility of directly retrieving the DSDs from polarimetric measurements based on the three-parameter GM was studied. The accuracy of the DSD model was determined by comparing the physical parameters (R, W, D_m, and N_t) estimated from polarimetric data with those calculated from the 2DVD observations. The results based on the C-G and EXP were used as references. It was found that the three-parameter GM was not suitable for directly retrieving DSDs from Z_H, Z_{DR}, and K_{DP}. Even if there was no error in the polarimetric data, the estimates still deviated from the truth because the three-parameter GM does not contain the statistical microphysical characteristics of the DSDs. When there were errors in the radar measurements, the retrievals based on the three-parameter GM were even worse. This unsatisfactory performance prevents the three-parameter GM from being used directly in the retrieval of DSDs. With some additional constraints (e.g., the μ–Λ relation), statistical DSD properties could be retained. Some other DSD models, for example, the generalized

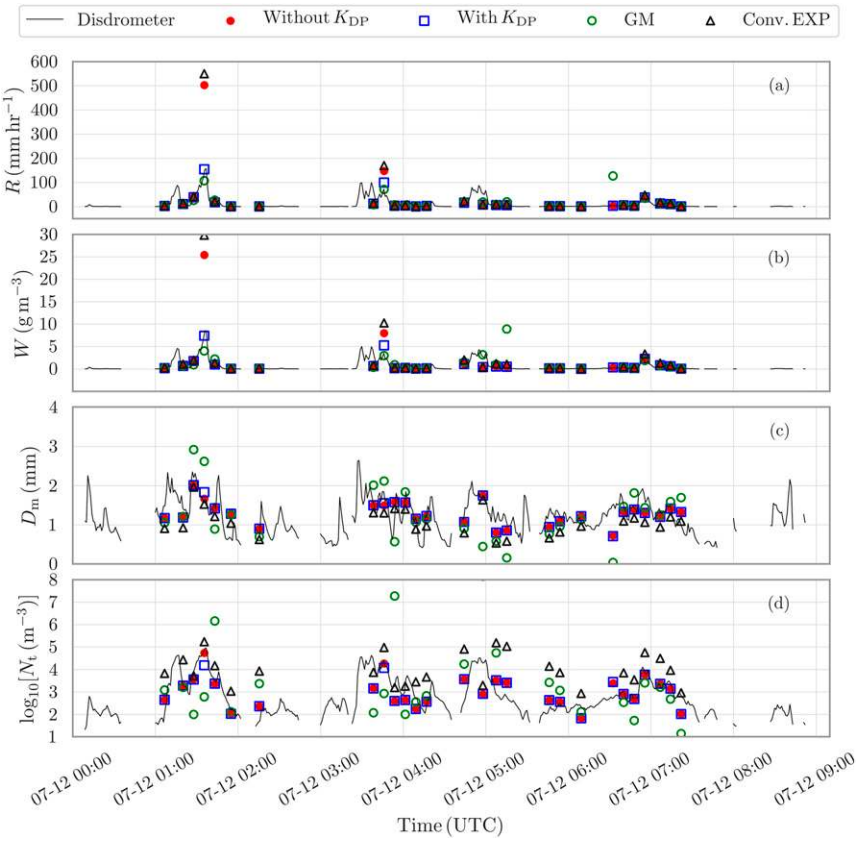

FIG. 11. Comparisons of radar retrieved (a) R, (b) W, (c) D_m, and (d) N_t with those calculated from the 2DVD data (black lines). The red dots and blue squares represent the results from EMA-based retrieval using C-G with/without K_{DP} measurements included. The green circles denote the results of EMA-based retrieval using the three-parameter GM and the black triangles denote the results of conventional retrieval using EXP.

gamma distribution with normalization (Lee et al. 2004; Thurai and Bringi 2018) and the gamma distribution constrained by a statistical D_m–σ_m relation (Williams et al. 2014; Zhang 2015), have similar effect.

From the comparisons of the estimated physical parameters with and without K_{DP} measurements used in the retrievals, it was found that the retrievals based on the EXP became worse when more information was used. Retrieval methods based on C-G could make full use of all the polarimetric measurements since the constraints of C-G suppressed the effect of K_{DP} errors and thus performed better than those only using the Z_H and Z_{DR} measurements. It was also demonstrated that, when errors were contained in K_{DP} measurements, the accuracy of W could be further enhanced when an accurate $\sigma_{K_{DP}}$ was used in the EMA, especially when $Z_H > 35$ dBZ. The $\sigma_{K_{DP}}$ term in the EMA indicates the reliability of K_{DP} measurements. If the K_{DP} is overly trusted ($\sigma_{K_{DP}}$ too small), measurement errors can reduce the accuracy of the estimates. On the other hand, if the $\sigma_{K_{DP}}$ values used are too large, the useful information in K_{DP} measurements cannot be efficiently utilized. It is therefore important to use an accurately estimated $\sigma_{K_{DP}}$ to obtain more accurate DSD estimates. The effects of the errors in Z_H and Z_{DR} measurements were not investigated but are expected to have similar effects.

Finally, polarimetric radar measurements and 2DVD observations from two precipitation events were used to verify the performance of these approaches. The retrieval using the three-parameter GM showed the lowest accuracy as compared with the other three approaches. When only Z_H and Z_{DR} were used in the EMA-based retrieval using C-G, R and W were sometimes substantially overestimated. However, the overestimation problem was solved by using all three measurements (Z_H, Z_{DR}, and K_{DP}) in retrievals, indicating the advantage of making full use of all available information. The conventional retrieval using EXP showed decreased

TABLE 3. The statistical comparisons of the radar-derived physical parameters (R, W, D_m, and N_t) and the 2DVD observations in two real events. Four methods were included for comparison (i.e., the EMA-based retrieval using C-G with and without the K_{DP} included, the EMA-based retrieval using the three-parameter GM, and the conventional retrieval using EXP).

		0000–0900 UTC 12 Jul 2014				1500 UTC 3 Jul–0600 UTC 5 Jul 2014			
		C-G with K_{DP}	C-G without K_{DP}	GM	Conventional EXP	C-G with K_{DP}	C-G without K_{DP}	GM	Conventional EXP
R (mm h^{-1})	CC	0.87	0.86	0.58	0.86	0.82	0.81	0.16	0.81
	FE	1.25	1.35	2.68	1.97	1.05	1.06	10.84	1.41
	RMSE	16.31	64.92	28.1	74.96	5.52	7.77	25.81	9.72
	BIAS	−1.53	10.92	0.68	15.12	0.82	1.15	7.28	2.19
W (g m^{-3})	CC	0.85	0.87	−0.06	0.87	0.78	0.78	−0.07	0.72
	FE	1.34	1.43	65.85	2.91	1.12	1.13	408.43	2.14
	RMSE	0.91	3.2	73.08	4.14	0.31	0.42	81.61	0.7
	BIAS	−0.06	0.59	13.08	1.05	0.06	0.08	19.17	0.23
D_m (mm)	CC	0.59	0.59	0.48	0.66	0.51	0.51	0.33	0.49
	FE	0.22	0.22	0.34	0.29	0.23	0.23	0.37	0.24
	RMSE	0.32	0.32	0.58	0.42	0.3	0.3	0.56	0.37
	BIAS	−0.09	−0.1	−0.15	−0.31	0.01	0.01	−0.14	−0.19
$\log_{10}[N_t]$	CC	0.54	0.58	0.04	0.23	0.53	0.53	0.02	0.34
	FE	0.18	0.17	0.54	0.41	0.18	0.18	0.72	0.38
	RMSE	7	6.86	23.91	13.14	5.71	5.72	30.19	11.79
	BIAS	−1.35	−1.13	6.41	9.12	−1.11	−1.1	11.67	8.63

performance because that the model was not tuned for the specific research region and that the measured information was not fully utilized.

The performance of the DSD models depends on what physical parameters we are interested in. For example, besides W, R, D_m, and N_t, reflectivity (Z, sixth moment of DSD) was also calculated from the DSDs to evaluate the performance of different models. No matter which model was used, all the retrieved Z values were generally close to the real values in all the experiments in sections 2 and 3. This is mainly because the Z_H measurements are close to the sixth moment of DSD. The retrieval of Z suffered less from the truncation errors and the measurement errors, and the impact of the DSD models was minor. Thus, when evaluating the other DSD models for retrieval, further experiments should be done through comparisons on the physical parameters of interest.

In the above analysis, the gamma distribution constrained by a statistical μ–Λ relation (C-G) had advantages over the unconstrained-gamma distribution in DSD retrieval. However, the C-G also had its own disadvantage because the determination of an accurate statistical μ–Λ relation is not easy. The μ and Λ are not DSD moments and are usually determined by the moment-fitting method (Vivekanandan et al. 2004). Since the DSD moments suffers from the sampling errors of 2DVD (Tokay et al. 2001, 2013, 2014; Thurai et al. 2017), the values of μ and Λ can be biased. To reduce the effect of sampling errors, the moments of median orders were used in estimation of the DSD parameters (the moment-fitting method; Cao and Zhang 2009).The method of sorting and averaging based on two parameters (SATP) might also be a way to mitigate the sampling errors (Cao et al. 2008). Since the sampling errors cannot be completely eliminated by this method, the only way is to minimize its effect as much as possible. In addition, due to the limits of Λ (less than 20) used in the EMA analysis, there was a lower limit for D_m (about 0.7 mm) for the retrieval based on the C-G. In the DSD dataset (21 739 samples) used for simulation, there were 3088 DSD samples (about 14%) with D_m values less than 0.7 mm. Within these samples, only 967 (about 4%) samples showed larger differences (>0.2 mm) from the D_m estimated based on the C-G model in the simulation experiment with no measurement errors assumed (Fig. 2). Thus, the lower limit due to the C-G model was acceptable considering the other advantages of the C-G.

In addition, explicitly constraining the DSD models by fixed relations is not the only way to introduce physical constraints to retrievals. Based on the Bayesian theorem, the climatic information of the DSD parameters (N_0 and Λ) was used to obtain better DSD estimates by Cao et al. (2010). Similarly, climatic statistics of N_0, μ, and Λ can be added to the EMA as a priori information to constrain the retrieval, in which the EMA becomes the variational analysis, which is a potential way to obtain accurate DSD estimates on the basis of the three-parameter GM. In addition, an extra term, which adjusts the DSD parameters to a statistical constraint (e.g., the μ–Λ relation), may be included in the cost function of EMA or a variational analysis. On the other hand, it is

not necessary to calculate K_{DP} from Φ_{DP} measurements before the DSD retrieval. The Φ_{DP} measurements can be directly used if the DSDs in a ray are simultaneously retrieved based on the EMA or a variational analysis.

In the future, a promising way to retrieve DSDs could be to use all the available information, including climatology statistics, all measurements, time evolution of the weather systems, spatiotemporal continuities of precipitation properties, and physical constraints in a statistics-based framework (e.g., EMA, variational analysis) or the Bayesian theorem–based analysis. With the correct characterization of the uncertainties of these sources of information, the DSD parameters and the corresponding physical parameters can be optimized.

Acknowledgments. The authors thank the scientists and engineers working on the 2DVD, Lishui radar, and the other instruments. The authors also thank Dr. Yinghui Lu (PSU) for his careful proofreading of this manuscript. This work was supported by the National Key Research and Development Program of China (Grants 2017YFC1501703 and 2018YFC1506404), the National Natural Science Foundation of China (Grants 41475015, 41875053, and 41675023), the Open Research Program of the State Key Laboratory of Severe Weather, and the Key Research Development Program of Jiangsu Science and Technology Department (Social Development Program, BE2016732).

APPENDIX

The EMA-Based DSD Retrieval

Measurements of polarimetric variables can be outside the variables' physical bounds, due to measurement errors. For these measurements, no valid estimates can be obtained using the explicit equation-solving approaches. Extra considerations are required for this kind of problem. The algorithms based on forward operators, which calculate polarimetric variables from DSDs, are suitable for dealing with measurement errors (Rodgers 2000); see Eqs. (1)–(3). Physical constraints are implied in the forward operators, and they help to eliminate the effects of erroneous measurements. Bayesian theory and its variant variational analysis are usually used together with the forward operators to optimally estimate DSDs. Because we did not consider the a priori information in our retrieval, a variant of the variational analysis method was used as a general method for DSD retrieval in this study. In this method, any one of the three-parameter GM, EXP, and C-G distributions can be used as the DSD model. The basic concept can be interpreted as follows. The a priori term in the variational analysis is omitted in the variant and we refer to it as the EMA approach.

First assume a DSD model, the three-parameter GM, EXP, or C-G. Then the DSD parameters are denoted with a state vector $\mathbf{x}$, $\mathbf{x} = [N_0, \Lambda]^T$ for EXP and C-G and $\mathbf{x} = [N_0, \Lambda, \mu]^T$ for the three-parameter GM. The superscript T means a transpose. The state vector $\mathbf{x}$ is optimized when the cost function is minimized:

$$J(\mathbf{x}) = \frac{1}{2}[H(\mathbf{x}) - \mathbf{y}]^T \mathbf{R}^{-1}[H(\mathbf{x}) - \mathbf{y}], \tag{A1}$$

where the forward operators are represented by $H(\cdot)$, which predicts the polarimetric variables Z_H, Z_{DR}, and K_{DP} from $\mathbf{x}$; $\mathbf{y}$ is the observation vector $[Z_H, Z_{DR}, \text{or } K_{DP}]^T$; and $\mathbf{R}$ is the error covariance of $\mathbf{y}$. In this study, we assumed the errors in Z_H, Z_{DR}, and K_{DP} were independent and $\mathbf{R}$ was diagonal (Cao et al. 2010), which was expressed as

$$\mathbf{R} = \begin{bmatrix} \sigma^2_{Z_H} & 0 & 0 \\ 0 & \sigma^2_{Z_{DR}} & 0 \\ 0 & 0 & \sigma^2_{K_{DP}} \end{bmatrix}, \tag{A2}$$

where σ_{Z_H}, $\sigma_{Z_{DR}}$, and $\sigma_{K_{DP}}$ are the standard deviations of the errors in Z_H, Z_{DR}, and K_{DP}. The forward model $H(\cdot)$ first calculates $N(D)$ from $\mathbf{x}$ based on the assumed DSD model, and then calculates Z_H, Z_{DR}, and K_{DP} using Eqs. (1)–(3). To minimize Eq. (A1), its corresponding gradient is given by

$$\mathbf{g}(\mathbf{x}) = \mathbf{H}^T \mathbf{R}^{-1}[H(\mathbf{x}) - \mathbf{y}], \tag{A3}$$

where $\mathbf{H}$ is the Jacobian matrix composed of the partial derivative of the predicted variables. As we know, the forward operators are nonlinear, so $\mathbf{x}$ is minimized iteratively using the linearized forward operators $H(\mathbf{x}) = H(\mathbf{x}_k) + H^T \times (\mathbf{x} - \mathbf{x}_k)$, where the subscript of $\mathbf{x}$ means $\mathbf{x}$ at the kth iteration. By setting the gradient to zero, the optimized $\mathbf{x}$, which minimizes the linearized cost function at the k + first iteration, is given by

$$\mathbf{x}_{k+1} = \mathbf{x}_k + \mathbf{A}^{-1}(\mathbf{H}^T \mathbf{R}^{-1} \delta \mathbf{y}), \tag{A4}$$

where $= \mathbf{H}^T \mathbf{R}^{-1} \mathbf{H}$, and $\delta \mathbf{y} = \mathbf{y} - H(\mathbf{x})$. We use $N_0 = 8 \times 10^3\ \text{m}^{-3}\ \text{mm}^{-1}$, $\Lambda = 5\ \text{mm}^{-1}$, and $\mu = 0$ for the first iteration. Note that the optimization method is not very sensitive to the choice of these values. A χ^2 convergence test can be used for the termination of the iteration. In this study, we used another way to solve the problem, which was to minimize Eq. (A1) directly using the bounded nonlinear optimization algorithm, for example, the limited-memory Broyden–Fletcher–Goldfarb–Shanno algorithm for bound-constrained large-scale

nonlinear optimization (L-BFGS-B; Byrd et al. 1995). With Eqs. (A1) and (A3), the Hessian is approximately estimated with the optimization procedures. One of the advantages of these bounded optimization algorithms is their ability to constrain the DSD parameter solutions within given upper and lower limits to avoid solutions without a physical meaning. The limits for the DSD parameters used in this study were $10^{-4} \le N_0 \le 10^{15}$, $0.01 \le \Lambda \le 20$, and $-3.5 \le \mu \le 15$ (Cao et al. 2008). The DSD parameters and $N(D)$ were considered to be statistically optimized when the state variable $\mathbf{x}$ minimized Eq. (A1) (Rodgers 2000). Note that, for C-G and EXP, Z_{DR} monotonically changes with Λ; Z_H and K_{DP} monotonically change with Λ (N_0) if N_0 (Λ) is fixed. Thus, there is a one-to-one mapping between the DSD parameter sets and the polarimetric variables. In such a case, the cost function is concave and EMA analysis can always reach global minimization. For the three-parameter GM, similar monotonic relationships between the polarimetric variables and DSD parameters generally exist except when K_{DP} (Z_{DR}) is close to $0^\circ\,km^{-1}$ (0 dB). When K_{DP} (Z_{DR}) is close to $0^\circ\,km^{-1}$ (0 dB), nonmonotonicity can exist. Thus, the cost function is linearized and converted to a quadratic function in this study, which helps to avoid the local minimization.

One of the keys for EMA-based retrieval is its error terms (σ_{Z_H}, $\sigma_{Z_{DR}}$, and $\sigma_{K_{DP}}$). They denote the reliability of the measurements. If we assume no errors exist in the polarimetric data, the corresponding error terms should be very small, for example, $\sigma_{Z_H} = 0.0001$ dB, $\sigma_{Z_{DR}} = 0.000\,02$ dB, and $\sigma_{K_{DP}} = 0.000\,03^\circ\,km^{-1}$. For practical applications, the error terms denote the measurement errors, which are mainly decided from the radar digital signal processing or estimation processes. If one of the error terms is enlarged, the corresponding polarimetric measurements are less trusted and less information is contained in the results.

REFERENCES

Anagnostou, M. N., J. Kalogiros, F. S. Marzano, E. N. Anagnostou, M. Montopoli, and E. Piccioti, 2013: Performance evaluation of a new dual-polarization microphysical algorithm based on long-term X-band radar and disdrometer observations. *J. Hydrometeor.*, **14**, 560–576, https://doi.org/10.1175/JHM-D-12-057.1.

Brandes, E. A., G. Zhang, and J. Vivekanandan, 2002: Experiments in rainfall estimation with a polarimetric radar in a subtropical environment. *J. Appl. Meteor.*, **41**, 674–685, https://doi.org/10.1175/1520-0450(2002)041<0674:EIREWA>2.0.CO;2.

——, ——, and ——, 2004a: Drop size distribution retrieval with polarimetric radar: Model and application. *J. Appl. Meteor.*, **43**, 461–475, https://doi.org/10.1175/1520-0450(2004)043<0461:DSDRWP>2.0.CO;2.

——, ——, and ——, 2004b: Comparison of polarimetric radar drop size distribution retrieval algorithms. *J. Atmos. Oceanic Technol.*, **21**, 584–598, https://doi.org/10.1175/1520-0426(2004)021<0584:COPRDS>2.0.CO;2.

Bringi, V. N., and V. Chandrasekar, 2001: *Polarimetric Doppler Weather Radar: Principles and Applications*. Cambridge University Press, 664 pp.

——, G.-J. Huang, V. Chandrasekar, and E. Gorgucci, 2002: A methodology for estimating the parameters of a gamma raindrop size distribution model from polarimetric radar data: Application to a squall-line event from the TRMM/Brazil campaign. *J. Atmos. Oceanic Technol.*, **19**, 633–645, https://doi.org/10.1175/1520-0426(2002)019<0633:AMFETP>2.0.CO;2.

——, L. Tolstoy, M. Thurai, and W. A. Petersen, 2015: Estimation of spatial correlation of drop size distribution parameters and rain rate using NASA's S-band polarimetric radar and 2D video disdrometer network: Two case studies from MC3E. *J. Hydrometeor.*, **16**, 1207–1221, https://doi.org/10.1175/JHM-D-14-0204.1.

Byrd, R. H., P. Lu, J. Nocedal, and C. Zhu, 1995: A limited memory algorithm for bound constrained optimization. *SIAM J. Sci. Comput.*, **16**, 1190–1208, https://doi.org/10.1137/0916069.

Cao, Q., and G. Zhang, 2009: Errors in estimating raindrop size distribution parameters employing disdrometer and simulated raindrop spectra. *J. Appl. Meteor. Climatol.*, **48**, 406–425, https://doi.org/10.1175/2008JAMC2026.1.

——, ——, E. Brandes, T. Schuur, A. Ryzhkov, and K. Ikeda, 2008: Analysis of video disdrometer and polarimetric radar data to characterize rain microphysics in Oklahoma. *J. Appl. Meteor. Climatol.*, **47**, 2238–2255, https://doi.org/10.1175/2008JAMC1732.1.

——, ——, ——, and ——, 2010: Polarimetric radar rain estimation through retrieval of drop size distribution using a Bayesian approach. *J. Appl. Meteor. Climatol.*, **49**, 973–990, https://doi.org/10.1175/2009JAMC2227.1.

——, M. B. Yeary, and G. Zhang, 2012: Efficient ways to learn weather radar polarimetry. *IEEE Trans. Educ.*, **55**, 58–68, https://doi.org/10.1109/TE.2011.2118211.

Doviak, R. J., and D. S. Zrnić, 1993: *Doppler Radar and Weather Observations*. 2nd ed. Academic Press, 562 pp.

Giangrande, S. E., R. McGraw, and L. Lei, 2013: An application of linear programming to polarimetric radar differential phase processing. *J. Atmos. Oceanic Technol.*, **30**, 1716–1729, https://doi.org/10.1175/JTECH-D-12-00147.1.

Gorgucci, E., V. Chandrasekar, V. N. Bringi, and G. Scarchilli, 2002: Estimation of raindrop size distribution parameters from polarimetric radar measurements. *J. Atmos. Sci.*, **59**, 2373–2384, https://doi.org/10.1175/1520-0469(2002)059<2373:EORSDP>2.0.CO;2.

Gosset, M., E.-P. Zahiri, and S. Moumouni, 2010: Rain drop size distribution variability and impact on X-band polarimetric radar retrieval: Results from the AMMA campaign in Benin. *Quart. J. Roy. Meteor. Soc.*, **136**, 243–256, https://doi.org/10.1002/qj.556.

Huang, H., G. Zhang, K. Zhao, and S. E. Giangrande, 2017: A hybrid method to estimate specific differential phase and rainfall with linear programming and physics constraints. *IEEE Trans. Geosci. Remote Sens.*, **55**, 96–111, https://doi.org/10.1109/TGRS.2016.2596295.

——, and Coauthors, 2018: Quantitative precipitation estimation with operational polarimetric radar measurements in southern China: A differential phase–based variational approach. *J. Atmos. Oceanic Technol.*, **35**, 1253–1271, https://doi.org/10.1175/JTECH-D-17-0142.1.

Kalogiros, J., M. N. Anagnostou, E. N. Anagnostou, M. Montopoli, E. Picciotti, and F. S. Marzano, 2013: Optimum estimation of rain microphysical parameters from X-band dual-polarization radar observables. *IEEE Trans. Geosci. Remote Sens.*, **51**, 3063–3076, https://doi.org/10.1109/TGRS.2012.2211606.

Kumjian, M. R., and A. V. Ryzhkov, 2010: The impact of evaporation on polarimetric characteristics of rain: Theoretical model and practical implications. *J. Appl. Meteor. Climatol.*, **49**, 1247–1267, https://doi.org/10.1175/2010JAMC2243.1.

——, and O. P. Prat, 2014: The impact of raindrop collisional processes on the polarimetric radar variables. *J. Atmos. Sci.*, **71**, 3052–3067, https://doi.org/10.1175/JAS-D-13-0357.1.

Lee, G. W., 2006: Sources of errors in rainfall measurements by polarimetric radar: Variability of drop size distributions, observational noise, and variation of relationships between R and polarimetric parameters. *J. Atmos. Oceanic Technol.*, **23**, 1005–1028, https://doi.org/10.1175/JTECH1899.1.

——, I. Zawadzki, W. Szyrmer, D. Sempere-Torres, and R. Uijlenhoet, 2004: A general approach to double-moment normalization of drop size distributions. *J. Appl. Meteor.*, **43**, 264–281, https://doi.org/10.1175/1520-0450(2004)043<0264:AGATDN>2.0.CO;2.

Maesaka, T., K. Iwanami, and M. Maki, 2012: Non-negative K_{DP} estimation by monotone increasing Φ_{DP} assumption below melting layer. Preprints, *Seventh European Conf. on Radar in Meteorology and Hydrology*, Toulouse, France, Météo France, 26 QPE.

Mishchenko, M. I., L. D. Travis, and D. W. Mackowski, 1996: *T*-matrix computations of light scattering by nonspherical particles: A review. *J. Quant. Spectrosc. Radiat. Transfer*, **55**, 535–575, https://doi.org/10.1016/0022-4073(96)00002-7.

Moisseev, D. N., and V. Chandrasekar, 2007: Examination of the μ–Λ relation suggested for drop size distribution parameters. *J. Atmos. Oceanic Technol.*, **24**, 847–855, https://doi.org/10.1175/JTECH2010.1.

Morrison, H., M. R. Kumjian, C. P. Martinkus, O. P. Prat, and M. van Lier-Walqui, 2019: A general *N*-moment normalization method for deriving rain drop size distribution scaling relationships. *J. Appl. Meteor. Climatol.*, **58**, 247–267, https://doi.org/10.1175/JAMC-D-18-0060.1.

Park, S. G., M. Maki, K. Iwanami, V. N. Bringi, and V. Chandrasekar, 2005: Correction of radar reflectivity and differential reflectivity for rain attenuation at X band. Part II: Evaluation and application. *J. Atmos. Oceanic Technol.*, **22**, 1633–1655, https://doi.org/10.1175/JTECH1804.1.

Raupach, T. H., and A. Berne, 2017: Retrieval of the raindrop size distribution from polarimetric radar data using double-moment normalisation. *Atmos. Meas. Tech.*, **10**, 2573–2594, https://doi.org/10.5194/amt-10-2573-2017.

Rodgers, C. D., 2000: *Inverse Methods for Atmospheric Sounding: Theory and Practice*. Series on Atmospheric, Oceanic and Planetary Physics, Vol. 2, World Scientific, 238 pp.

Ryzhkov, A. V., S. Giangrande, and T. Schuur, 2003: Rainfall measurements with the polarimetric WSR-88D radar. NOAA Rep., 99 pp.

Seliga, T. A., and V. N. Bringi, 1976: Potential use of radar differential reflectivity measurements at orthogonal polarizations for measuring precipitation. *J. Appl. Meteor.*, **15**, 69–76, https://doi.org/10.1175/1520-0450(1976)015<0069:PUORDR>2.0.CO;2.

Testud, J., S. Oury, R. A. Black, P. Amayenc, and X. Dou, 2001: The concept of ''normalized'' distribution to describe raindrop spectra: A tool for cloud physics and cloud remote sensing. *J. Appl. Meteor.*, **40**, 1118–1140, https://doi.org/10.1175/1520-0450(2001)040<1118:TCONDT>2.0.CO;2.

Thurai, M., and V. N. Bringi, 2018: Application of the generalized gamma model to represent the full rain drop size distribution spectra. *J. Appl. Meteor. Climatol.*, **57**, 1197–1210, https://doi.org/10.1175/jamc-d-17-0235.1.

——, P. Gatlin, V. N. Bringi, W. Petersen, P. Kennedy, B. Notaroš, and L. Carey, 2017: Toward completing the raindrop size spectrum: Case studies involving 2D-video disdrometer, droplet spectrometer, and polarimetric radar measurements. *J. Appl. Meteor. Climatol.*, **56**, 877–896, https://doi.org/10.1175/JAMC-D-16-0304.1.

Tokay, A., A. Kruger, and W. F. Krajewski, 2001: Comparison of drop size distribution measurements by impact and optical disdrometers. *J. Appl. Meteor.*, **40**, 2083–2097, https://doi.org/10.1175/1520-0450(2001)040<2083:CODSDM>2.0.CO;2.

——, W. A. Petersen, P. Gatlin, and M. Wingo, 2013: Comparison of raindrop size distribution measurements by collocated disdrometers. *J. Atmos. Oceanic Technol.*, **30**, 1672–1690, https://doi.org/10.1175/JTECH-D-12-00163.1.

——, D. B. Wolff, and W. A. Petersen, 2014: Evaluation of the new version of the laser-optical disdrometer, OTT Parsivel^2. *J. Atmos. Oceanic Technol.*, **31**, 1276–1288, https://doi.org/10.1175/JTECH-D-13-00174.1.

Ulbrich, C. W., 1983: Natural variations in the analytical form of the raindrop size distribution. *J. Climate Appl. Meteor.*, **22**, 1764–1775, https://doi.org/10.1175/1520-0450(1983)022<1764:NVITAF>2.0.CO;2.

Vivekanandan, J., W. M. Adams, and V. N. Bringi, 1991: Rigorous approach to polarimetric radar modeling of hydrometeor orientation distributions. *J. Appl. Meteor.*, **30**, 1053–1063, https://doi.org/10.1175/1520-0450(1991)030<1053:RATPRM>2.0.CO;2.

——, G. Zhang, S. M. Ellis, D. Rajopadhyaya, and S. K. Avery, 2003: Radar reflectivity calibration using differential propagation phase measurement. *Radio Sci.*, **38**, 14, https://doi.org/10.1029/2002RS002676.

——, ——, and E. Brandes, 2004: Polarimetric radar estimators based on a constrained gamma drop size distribution model. *J. Appl. Meteor.*, **43**, 217–230, https://doi.org/10.1175/1520-0450(2004)043<0217:PREBOA>2.0.CO;2.

Wen, L., K. Zhao, G. Zhang, M. Xue, B. Zhou, S. Liu, and X. Chen, 2016: Statistical characteristics of raindrop size distributions observed in East China during the Asian summer monsoon season using 2-D video disdrometer and Micro Rain Radar data. *J. Geophys. Res. Atmos.*, **121**, 2265–2282, https://doi.org/10.1002/2015JD024160.

Williams, C. R., and Coauthors, 2014: Describing the shape of raindrop size distributions using uncorrelated raindrop mass spectrum parameters. *J. Appl. Meteor. Climatol.*, **53**, 1282–1296, https://doi.org/10.1175/JAMC-D-13-076.1.

Zhang, G., 2015: Comments on ''Describing the shape of raindrop size distributions using uncorrelated raindrop mass spectrum parameters.'' *J. Appl. Meteor. Climatol.*, **54**, 1970–1976, https://doi.org/10.1175/JAMC-D-14-0210.1.

——, 2016: *Weather Radar Polarimetry*. 1st ed. CRC Press, 322 pp.

——, J. Vivekanandan, and E. Brandes, 2001: A method for estimating rain rate and drop size distribution from polarimetric radar measurements. *IEEE Trans. Geosci. Remote Sens.*, **39**, 830–841, https://doi.org/10.1109/36.917906.

——, ——, ——, R. Meneghini, and T. Kozu, 2003: The shape–slope relation in observed gamma raindrop size distributions: Statistical error or useful information? *J. Atmos. Oceanic Technol.*, **20**, 1106–1119, https://doi.org/10.1175/1520-0426(2003)020<1106:TSRIOG>2.0.CO;2.

——, J. Sun, and E. A. Brandes, 2006: Improving parameterization of rain microphysics with disdrometer and radar observations. *J. Atmos. Sci.*, **63**, 1273–1290, https://doi.org/10.1175/JAS3680.1.